BBA - Molecular Basis of Disease xxx (xxxx) xxxx

Contents lists available at ScienceDirect

BBA - Molecular Basis of Disease

journal homepage: www.elsevier.com/locate/bbadis

Mitochondrial remodeling in human skin fibroblasts from sporadic male Parkinson's disease patients uncovers metabolic and mitochondrial bioenergetic defects

Cláudia M. Deus[a,b], Susana P. Pereira[a,b,c], Teresa Cunha-Oliveira[a], Francisco B. Pereira[d,e], Nuno Raimundo[f], Paulo J. Oliveira[a,b,*]

[a] CNC - Center for Neuroscience and Cell Biology, University of Coimbra, UC Biotech, Biocant Park, 3060-197 Cantanhede, Portugal
[b] IIIUC - Institute for Interdisciplinary Research, University of Coimbra, 3030-789 Coimbra, Portugal
[c] LaMetEx - Laboratory of Metabolism and Exercise, Research Centre in Physical Activity, Health and Leisure (CIAFEL), Faculty of Sport, University of Porto, 4200-450 Porto, Portugal
[d] Center for Informatics and Systems, University of Coimbra, Polo II, Pinhal de Marrocos, 3030-290 Coimbra, Portugal
[e] Coimbra Polytechnic - ISEC, 3030-193 Coimbra, Portugal
[f] Institute of Cellular Biochemistry, University Medical Center Goettingen, Humboldtallee 23, D-37073 Goettingen, Germany

ARTICLE INFO

Keywords:
Human skin fibroblasts
metabolism
mitochondria
mitochondrial remodeling
personalized medicine
sporadic Parkinson's disease

ABSTRACT

Parkinson's Disease (PD) is characterized by dopaminergic neurodegeneration in the *substantia nigra*. The exact mechanism by which dopaminergic neurodegeneration occurs is still unknown; however, mitochondrial dysfunction has long been implicated in PD pathogenesis. To investigate the sub-cellular events that lead to disease progression and to develop personalized interventions, non-neuronal cells which are collected in a minimally invasive manner can be key to test interventions aimed at improving mitochondrial function. We used human skin fibroblasts from sporadic PD (sPD) patients as a cell proxy to detect metabolic and mitochondrial alterations which would also exist in a non-neuronal cell type. In this model, we used a glucose-free/galactose- glutamine- and pyruvate-containing cell culture medium, which forces cells to be more dependent on oxidative phosphorylation (OXPHOS) for energy production, in order to reveal hidden metabolic and mitochondrial alterations present in fibroblasts from sPD patients.

We demonstrated that fibroblasts from sPD patients show hyperpolarized and elongated mitochondrial networks and higher mitochondrial ROS concentration, as well as decreased ATP levels and glycolysis-related ECAR. Our results also showed that abnormalities of fibroblasts from sPD patients became more evident when stimulating OXPHOS. Under these culture conditions, fibroblasts from sPD cells presented decreased basal respiration, ATP-linked OCR and maximal respiration, and increased mitochondria-targeting phosphorylation of DRP1 when compared to control cells.

Our work validates the relevance of using fibroblasts from sPD patients to study cellular and molecular changes that are characteristic of dopaminergic neurodegeneration of PD, and shows that forcing mitochondrial OXPHOS uncovers metabolic defects that were otherwise hidden.

1. Introduction

Parkinson's Disease (PD) is a progressive degenerative disorder of the central nervous system that mainly affects the motor system. In fact, PD is the most common movement disorder and the second most common neurodegenerative disorder after Alzheimer's disease (AD), showing a prevalence of 2–3% in people older than 65 years old [1]. Besides age, sex is also a major PD risk factor, since PD incidence is 1.5 times higher in men than women [2].

According to its origin, parkinsonism can be divided into two main subtypes: a) idiopathic or sporadic, which is defined as a phenotype with unknown or no external identifiable causes, and b) hereditary or familial, which is defined as a phenotype caused by specific gene mutations [3]. However, only a small proportion of the PD cases results from genetic mutations, while around 85–90% of the cases are sporadic [4]. Notwithstanding, the majority of ex-vivo studies that investigate

* Corresponding author at: CNC - Center for Neuroscience and Cell Biology, University of Coimbra, UC Biotech, Lot 8A, Biocant Park, 3060-197 Cantanhede, Portugal.
E-mail addresses: xico@dei.uc.pt (F.B. Pereira), nuno.raimundo@med.uni-goettingen.de (N. Raimundo), pauloliv@cnc.uc.pt (P.J. Oliveira).

https://doi.org/10.1016/j.bbadis.2019.165615
Received 13 August 2019; Received in revised form 24 October 2019; Accepted 15 November 2019

PD etiopathogenesis have used human skin fibroblasts from hereditary PD patients [5–8].

Parkinson's Disease is characterized by dopaminergic neurodegeneration in *substantia nigra pars compacta*, culminating in decreased levels of dopamine in striatum [9]. The exact mechanism by which dopaminergic cell neurodegeneration occurs is still unknown; however, there are several mechanisms described that contribute to PD pathogenesis [10]. Current evidence suggests that mitochondrial impairment is a hallmark of PD [11]. Mitochondrial complex I inhibitors were previously described to cause nigrostriatal degeneration and parkinsonism [12]. In fact, rotenone, an inhibitor of mitochondrial complex I, has been extensively used as a model of PD, since it is able to reproduce pathological hallmarks of the disease, as well as motor coordination deficiency [13]. Moreover, it has also been established that oxidative stress, dysregulation in ubiquitin-proteasome system (UPS) and autophagy contributed to neuronal death in PD [14].

Some studies used peripheral tissues, namely skin fibroblasts, as a reliable source of biological tissue that could reflect the metabolic changes in neuronal cells [5,14,15]. Fibroblasts are accessible cells, which could be collected from PD patients in a minimally-invasive manner, retaining specific environmental and aging history, as well as polygenic risk factors from the patients allowing for a reliable model to study the pathogenesis of PD [16].

Currently, PD has no cure and no early diagnostics methods exist. To identify sub-cellular mechanisms of PD progression and develop a personalized medicine approach to PD, one needs to identify and validate cell systems that can be used to test interventions aimed at specific targets, one of them being mitochondrial function. Within this framework, our current hypotheses are that: a) human skin fibroblasts from sporadic PD (sPD) patients represent a minimally-invasive model to detect metabolic and mitochondrial alterations characteristic in PD patients and b) forcing mitochondrial oxidative phosphorylation (OXPHOS) in fibroblasts from sPD patients reveals hidden metabolic alterations.

Our work highlights the importance of using fibroblasts from sPD patients to study cellular and molecular changes, which are characteristic of dopaminergic neurodegeneration of PD, as well as a new strategy to identify cell proxies that can be used for an early diagnosis of PD.

2. Materials and methods

2.1. Reagents

Bovine serum albumin (BSA), ammonium persulfate (APS), Bradford reagent, brilliant blue G, calcium chloride ($CaCl_2$), dimethyl sulfoxide (DMSO), ethylenediaminetetraacetic acid (EDTA), glycerol, glycine, β-mercaptoethanol 98%, phenylmethylsulfonyl fluoride (PMSF), sodium chloride (NaCl), sodium dodecyl sulfate (SDS), sulforhodamine B sodium salt (SRB), trizma base, Tris pH 8.8, Tris pH 6.8, and trypan-blue solution were obtained from Sigma-Aldrich (Saint Louis, MO, USA). Acetic acid, ethanol, hydrochloric acid (HCl), magnesium chloride ($MgCl_2$), methanol, potassium chloride (KCl), potassium phosphate monobasic (KH_2PO_4), sodium hydrogencarbonate ($NaHCO_3$), sodium sulfate ($NaSO_4$), and sodium hydroxide (NaOH) were obtained from Merck (Whitehouse Station, NJ, USA). Acrylamide, Laemmli buffer, PVDF membranes, and *N,N,N′,N′*-Tetramethylethylenediamine (TEMED) were obtained from BioRad (Hercules, CA, USA). The ECF detection system was obtained from Healthcare Life Sciences (Buckinghamshire, UK). The fluorescent probes tetramethyl rhodaminemethylester (TMRM) and Hoechst 33342 were both obtained from Molecular Probes (Eugene, OR, USA). Dulbecco's modified Eagle's medium without glucose (DMEM, 5030), Earle's Balanced Salt Solution (EBSS, 14155063), penicillin, streptomycin, fetal bovine serum (FBS), and 0.25% Trypsin–EDTA were purchased from Gibco-Invitrogen (Grand Island, NY). Cell lysis buffer (9803) was obtained from Cell Signaling Technology (Danvers, MA, USA).

All reagents and chemical compounds used were of the greatest degree of purity commercially available. In the preparation of every solution, ultrapure distilled water (conductivity < 18 μS.cm-1), filtered by a Milli Q Millipore system, was always used in order to minimize as much as possible contamination with metal ions.

Table 1
Clinical information of human skin fibroblasts from sporadic Parkinson's disease patients and respective age- and sex-matched healthy controls.

	Controls patients (C)	Parkinson's disease patients (PD)
Sample size (n, males)	5	5
Age (years)	67.6 ± 3.7	62.6 ± 0.5
Race	Caucasian	Caucasian
Diagnostic age (years)		54.4 ± 3.7
Onset age (years)		52.6 ± 3.4
Mini-mental state examination score (MMSE)	28.3 ± 1.2	29.4 ± 0.4
Hoehn and Yahr stage (1 until 5)		1.4 ± 0.2

Values are expressed as a mean ± standard error of the mean (SEM).

2.2. Cell culture conditions

Skin fibroblasts from five sporadic late-onset PD male patients and five age- and sex-matched healthy controls (Table 1) were obtained from a cell line repository of Coriell Institute for Medical Research, USA (www.coriell.org). Inclusion criteria to choose skin fibroblasts from sPD patients and their respective age- and sex-matched controls were: a) samples from male individuals (since PD incidence is 1.5 times higher in men than women [2]), b) ages around 60–70 years old, c) absence of characteristic genetic mutations and d) clinical diagnostics of sporadic late-onset PD (85–90% of the PD cases are sporadic [4]). Other details as familial disease history, and lifestyle habits including smoking or exercise practice, were also taken into consideration to keep the variables more similar between patients and healthy controls. As described by the supplier, all fibroblast cell lines were isolated from skin biopsies of the upper medial arm and cultured under highly standardized conditions. In our laboratory, fibroblasts from sPD patients were cultured in DMEM (D5030) supplemented with 4.5 g/L (high-glucose medium, HGm), 1.8 g/L sodium bicarbonate, 0.11 g/L sodium pyruvate, 100 U/mL of penicillin, 100 g/mL of streptomycin, and 10% fetal bovine serum in tissue-culture dishes at 37 °C in a humidified atmosphere of 5% CO_2. Another group of cells were cultured in DMEM (D5030) supplemented with 0.9 g/L (Glucose medium, Gm), 1.8 g/L sodium bicarbonate, 0.11 g/L sodium pyruvate, 100 U/mL of penicillin, 100 g/mL of streptomycin, and 10% fetal bovine serum and 1, 6, and 24 h after seeding, cell culture medium was changed to galactose/glutamine/pyruvate-containing medium (OXPHOSm) or adapted for at least 5 passages before the experiments in a Dulbecco's Modified Eagle's Medium (DMEM, 5030) without glucose and supplemented with 1.8 g/L sodium bicarbonate, 0.11 g/L sodium pyruvate, 1.8 g/L galactose, 0.584 g/L L-glutamine, 100 U/mL of penicillin, 100 lg/mL of streptomycin, and 10% fetal bovine serum with the same culture conditions described before. This culture medium was used to force cells to mostly rely on OXPHOS for ATP production [17,18] and is described here as OXPHOS medium (OXPHOSm). Cells were passaged by trypsinization using standard methods when reaching 70–80% confluence and all experiments were prepared from cultures in log-phase growth. Taking into account that cell passage number can affect cell phenotype and responses, all experiments were performed with cells from passage 6 to 15 and cell passage was maintained constantly between fibroblasts from sPD patients and their age- and sex-matched controls.

2.3. Cell proliferation measurements

The sulforhodamine B (SRB) assay was used to measure cellular growth, proliferation, and to detect the loss of cell mass as a consequence of rotenone cytotoxicity. For growth curves analysis, cells were seeded at densities of 1000, 2500, 5000, 10,000, 15,000, and 20,000 cells/cm^2 in 96-well plates, with a final volume of 100 μL per well and allowed to proliferate for 24, 48, 72 and 96 h. For rotenone cytotoxicity measurement, cells were seeded at a concentration of 15,000 cells/cm^2 in 96-well plates, with a final volume of 100 μL per well and allowed to proliferate for 24 h. Then, 0.3, 1, 3, 10, 30, and 100 μM rotenone was added to cells for 24 and 48 h. For proliferation rate measurement, cells were seeded at a concentration of 15,000 cells/cm^2 in 96-well plates, with a final volume of 100 μL per well and allowed to proliferate for 24, 48, 72, 96, 168, 192 and 216 h.

At specific time points, the incubation medium was removed, and cells were fixed in 1% acetic acid in ice-cold methanol for at least one day at −20 °C. Cells were then incubated with 0.05% (w/v) SRB reagent dissolved in 1% acetic acid for 1 h at 37 °C. Unbound dye was removed with 1% acetic acid. Dye bound to cell proteins was extracted with 10 mM Tris-base solution, pH 10. After SRB labeling, absorbance was measured in a Biotek Cytation 3 spectrophotometer (BioTek Instruments Inc., USA) at 510 nm and the amount of dye released is proportional to the number of cells in each well [19,20]. A linear regression analysis for each cell line during 9 days using SRB values was calculated and the slope was used to estimate proliferation rate.

2.4. Cell viability measurements

The resazurin assay was used to measure the cellular viability based on metabolic activity of living cells through the fluorescence intensity. Cells were seeded at a concentration of 15,000 cells/cm^2 in 96-well plates, with a final volume of 100 μL per well. Resazurin stock solution (1 mg/mL) was prepared in PBS 1× and stored at −20 °C. After 24 h, cell medium from each well was removed and cells were washed with PBS 1×. After removing PBS 1×, 100 μL of resazurin solution (1:1000 dilution in growth medium from a stock solution) was added in each well and incubated for 5 h at 37 °C with a 5% CO_2 atmosphere. Resazurin is irreversibly converted into resorufin, whose fluorescence was next measured in a Biotek Cytation 3 spectrophotometer (BioTek Instruments Inc., USA) at 540/590 nm [19].

2.5. Adenosine triphosphate (ATP) level measurements

Intracellular ATP levels were measured by using CellTiter-Glo Luminescent Cell Viability Assay (G7571, Promega) following manufacturer's instructions. Human skin fibroblasts were seeded at a concentration of 15,000 cells/cm^2 in white opaque-bottom, 96-well plates, with a final volume of 100 μL per well. After 24 h, 50 μL of cell culture medium was removed and 50 μL CellTiter-Glo® Reagent (CellTiter-Glo Buffer + CellTiter-Glo Substrate) was added to the cells. Contents were mixed for 2 min on an orbital shaker to induce cell lysis and, after 10 min of incubation at 22 °C, the luminescence signal was monitored in a Biotek Cytation 3 spectrophotometer (BioTek Instruments Inc., USA). ATP standard curve was also generated following manufacturer's instructions. The luminescence signal was proportional to the amount of ATP present in the solution [21].

2.6. Mitochondrial network characterization by vital epifluorescence microscopy

Vital epifluorescence microscopy was used to detect alterations in mitochondrial polarization and network distribution in human skin fibroblasts by using the mitochondrial membrane potential-dependent (Δψmt) dye TMRM. Cells were seeded at a concentration of 7500 cells/cm^2 in black clear-bottom 24-well plates, with a final volume of 500 μL per well. Twenty-four hours after, cells were incubated with the fluorescent probes, TMRM (100 nM) and Hoescht 33324 (1 mg/mL) in microscopy solution buffer (120 mM NaCl, 3.5 mM KCl, 0.4 mM NaH_2PO_4, 20 mM HEPES, 5 mM $NaHCO_3$, 1.2 mM Na_2SO_4, and 10 mM sodium pyruvate) supplemented with 1.2 mM $MgCl_2$ and 1.3 mM $CaCl_2$. Images were obtained using the In Cell Analyzer 2200 (GE, Healthcare) microscope and were treated with ImageJ 1.45S program.

2.7. Determination of mitochondrial morphology

To determine and quantify mitochondrial morphology, an Image J macro was used [22]. Pictures of human skin fibroblasts stained with TMRM were extracted to grayscale, inverted to show mitochondria-specific fluorescence as black pixels, and thresholded to optimally resolve individual mitochondria. The mean area/perimeter ratio was employed as an index of mitochondrial interconnectivity and inverse circularity used as a measure of mitochondrial network elongation.

2.8. Determination of mitochondrial superoxide anion

To evaluate the concentration of superoxide anion in mitochondria, we used MitoSOX fluorescent dye, which permeates live cells where it selectively accumulates by polarized mitochondria and is rapidly oxidized by superoxide anion but not by other reactive oxygen species (ROS) and reactive nitrogen species (RNS). Human skin fibroblast were seeded at a concentration of 15,000 cells/cm^2 in 96-well plates, with a final volume of 100 μL per well. Fluorescent probes, MitoSOX (5 μM) and Hoescht 33324 (1 mg/mL) in a microscopy solution buffer (120 mM NaCl, 3.5 mM KCl, 0.4 mM NaH_2PO_4, 20 mM HEPES, 5 mM $NaHCO_3$, 1.2 mM Na_2SO_4, and 10 mM sodium pyruvate) supplemented with 1.2 mM $MgCl_2$ and 1.3 mM $CaCl_2$ were added in each well and incubated for 20 min at 37 °C with a 5% CO_2 atmosphere. The fluorescence was measured every 2 min for 90 min in a Biotek Cytation 3 spectrophotometer (BioTek Instruments Inc., USA) at 510/580 nm. At the end of the experiment, incubation medium was removed, and cells were fixed in 1% acetic acid in ice-cold methanol for at least one day at −20 °C. Sulforhodamine B assay was used to evaluate cell mass as described above and to normalize results.

2.9. Measurement of total superoxide dismutase (SOD) activity

Total SOD activity was measured by using a SOD activity assay kit (SOD activity Enzo Life Sciences, USA) following manufacturer's instructions. Briefly, human skin fibroblasts were seeded at a concentration of 15,000 cells/cm^2 in tissue-culture dishes, with a final volume of 10 mL. After 24 h, cells were harvested, washed with ice-cold 1× PBS and lysed as described in kit protocol. Protein concentration was determined using the Bradford method [23]. Cell lysates of each sample or standards (25 μL) were incubated with 150 μL reaction mixture containing WST-1 and Xanthine oxidase and then xanthine solution was added. Formazan formation was measured for 10 min at 37 °C, and the absorbance was monitored at 450 nm in a Biotek Cytation 3 spectrophotometer (BioTek Instruments Inc., USA). SOD standard curve was also generated following manufacturer's instructions.

2.10. Measurement of reduced and oxidized glutathione levels

Total cellular GSH/GSSG ratio [24] was determined by a GSH/GSSG-Glo assay kit (V6611, Promega, USA) following manufacturer's instructions. Briefly, human skin fibroblasts were seeded at a concentration of 15,000 cells/cm^2 in white opaque-bottom, 96-well plates, with a final volume of 100 μL per well. Then, cell culture medium was removed and 50 μL of total glutathione or oxidized glutathione lysis reagents were added and were mixed for 5 min on an orbital shaker to induce cell lysis. After, 50 μL of luciferin generation reagent was added and incubated at 22 °C for 30 min. Lastly, 100 μL of luciferin detection

Table 2
Sequences of primers used for the analysis of mitochondrial DNA copy number and gene transcripts.

Gene	Accession number	Forward primer	Reverse primer
CytB	NC_012920 (14747-15887)	CCACCCCATCCAACATCTCC	GCGTCTGGTGAGTAGTGCAT
B2m	NC_000015	TGTTCCTGCTGGGTAGCTCT	CCTCCATGATGCTGCTTACA
NDUFA9	NM_005002	GCCTATCGATGGGTAGCAAGAG	TGAGTTCCAGTGGTGTTGCC
SDHA	NM_004168	CGGGTCCATCCATCGCATAAG	TATATGCCTGTAGGGTGGAACTGAA
CYTC	NM_018947	CGTTGAAAAGGGAGGCAAGC	TCCCCAGATGATGCCTTTGTTC
COX4i1	NM_001861	GAGAAAGTCGAGTTGTATCGCA	GCTTCTGCCACATGATAACGA
ATP5G1	NM_001002027	GGCTAAAGCTGGGAGACTGAAA	GTGGGAAGTTGCTGTAGGAAGG
NRF1	NM_005011	TTGAGTCTAATCCATCTATCCG	TACTTACGCACCACATTCTC
NFE2L2	NM_006164	AACTACTCCCAGGTTGCCCA	AGCAATGAAGACTGGGCTCTC
PINK1	NM_032409	TGTGGAACATCTCGGCAGGT	GGCTAGTTGCTTGGGACCTC
MFN1	NM_033540	AGTTGGAGCGGAGACTTAGCA	TTCTACCAGATCATCTTCAGTGGC
MFN2	NM_014874	AGCTACACTGGCTCCAACTG	AACCGGCTTTATTCCTGAGCA
SOD1	NM_000454	CGAGCAGAAGGAAAGTAATG	GGATAGAGGATTAAAGTGAGGA
SOD2	NM_000636	GAAGTTCAATGGTGGTGGTCAT	TTCCAGCAACTCCCCTTTGG
MRPL51	NM_016497	TCTCTTGGTGTGCCTAGATTGA	CACTCCGAACATGGCCCTTTT
HPRT1	NM_000194	CCCTGGCGTCGTGATTAGTG	CGAGCAAGACGTTCAGTCCT
C19orf74	NM_001256440	ATGGAGGGGAAGTACGTCATC	GAGGCGGTCAAACACAGAC
FAM57A	NM_024792	TGAGCACTCCGTTTGTGTCG	CGGCCATAGGACCAGTACAT

reagent was added and after 15 min of incubation at 22 °C, the luminescence signal was monitored in a Biotek Cytation 3 spectrophotometer (BioTek Instruments Inc., USA).

2.11. Protein evaluation by western blotting

To obtain total cellular extracts, all cells were harvested by trypsinization and washed once with PBS 1×. In order to collect the cells, two centrifugation steps were performed for 5 min at 1000 ×*g* (4 °C). The cellular pellet was resuspended in cell lysis buffer 1× (Bio-Rad, 9803) supplemented with 100 μM phenylmethylsulfonyl fluoride (PMSF). The protein concentration in cellular extracts was determined by the Bradford assay, using bovine serum albumin (BSA) as a standard [23]. Samples were sonicated and 20 μg of total protein extract was separated by electrophoresis in a 12% SDS-PAGE gel, after denaturation at 95 °C for 5 min in Laemmli buffer (Bio-Rad) and electrophoretically transferred to 0.45 μm PVDF membranes. After blocking with 5% milk in TBST (50 mM Tris–HCl, pH 8; 154 mM NaCl and 0.1% tween 20) for 2 h at room temperature, PVDF membranes were incubated overnight at 4 °C under constant agitation with primary antibodies against PINK1 (1:1000, Abcam), Parkin (1:1000, Abcam), FIS1 (1:1000, Santa Cruz), OPA1 (1:1000, Santa Cruz), p-DRP1 (ser637) (1:1000, Cell Signaling), and actin (1:5000, Millipore). Membranes were washed three times with TBST for 5 min and incubated with the correspondent alkaline phosphatase-conjugated secondary antibody, goat anti-mouse IgG (1:2500, Santa Cruz) and goat anti-rabbit IgG (1:2500, Santa Cruz) for 1 h at room temperature. Membranes were then incubated with the ECF detection system (from GE Healthcare, Piscataway, NJ) and imaged with the Biospectrum – Multispectral imaging system (UVP; LLC Upland, CA; Cambridge, UK). The densities of each band were calculated with ImageJ 1.45S program and normalized for the respective actin band density.

2.12. Cellular oxygen consumption measurements

Oxygen consumption was measured at 37 °C using a Seahorse XF^{e}96 Extracellular Flux Analyzer (Seahorse Bioscience, Germany) [25]. All cell lines were seeded under the same conditions described above at a density of 70,000 cells/cm^2 since the absolute rate of oxygen consumption was linearly related to the cell number between 30,000 and 100,000 cells/well. A XF^{e}96 sensor cartridge for each cell plate was placed in a 96-well calibration plate containing 200 μL/well calibration buffer and left to hydrate overnight at 37 °C. The cell culture medium from the plates was replaced the following day with 180 μL/well of pre-warmed, low-buffered, serum-free minimal DMEM (102353, Bioscience) medium, with the pH adjusted to 7.4 and incubated at 37 °C for 1 h to allow the temperature and pH of the medium to reach equilibrium before the first rate measurement. Oligomycin, FCCP, rotenone, and antimycin were prepared in DMSO and 2-DG was prepared in pre-warmed, low-buffered, serum-free minimal DMEM (102353, Bioscience) medium. For oxygen consumption rate (OCR) measurements, 3 μM oligomycin, 2 μM FCCP, and 2.5 μM rotenone plus 2.5 μM antimycin were injected into reagent delivery port A, B, and C, respectively. For extracellular acidification rate (ECAR), 10 mM glucose, 3 μM oligomycin, and 100 mM 2-DG were injected into reagent delivery port A, B, and C, respectively. Next, 20, 22, and 24 μL of compounds were pre-loaded into the ports respectively, of each well in the XF^{e}96 sensor cartridge. Three baseline rate measurements of OCR and ECAR were made using a 3 min mix, 5 min measure cycle. The compounds were then pneumatically injected by the XF^{e}96 Analyzer into each well, mixed, and measurements of OCR and ECAR made using a 3 min mix, 5 min measure cycle. In the end of the experiment, incubation medium was removed, and cells were fixed in 1% acetic acid in ice-cold methanol for at least one day at −20 °C. Sulforhodamine B assay was used to evaluate cell mass as described above to normalize results. Results were analyzed by using the Software Wave Desktop Version 2.2.

2.13. Analysis of mitochondrial DNA (mtDNA) copy number

Cells were collected and centrifuged at 2000 ×*g* for 5 min. The pellets were washed in 5 mL of PBS and the suspension was centrifuged at 2000 ×*g* for 5 min. The resulting pellets were stored at −80 °C until DNA extraction. Total DNA was extracted from cell pellets using the QIAamp DNA mini kit (Qiagen, Düsseldorf, Germany), following manufacturer's protocols, sonicated in a water bath for 10 min, and quantified using a Nanodrop 2000 (ThermoScientific, Waltham, MA, USA). RT-PCR was performed using the SsoFast Eva Green Supermix, in a CFX96 real time-PCR system (Bio-Rad, Hercules, CA, USA), with the primers defined in Table 2, at 500 nM. Amplification of 25 ng DNA was performed with an initial cycle of 2 min at 98 °C, followed by 40 cycles of 5 s at 98 °C and 5 s at 63 °C. The amplification specificity was assessed at the end of the amplification by a melting curve between 65 and 95 °C, using an increment of 0.5 °C in each step. At the end of each cycle, Eva Green fluorescence was recorded to enable determination of Cq. For each set of primers, amplification efficiency was assessed, and no template controls were run. mtDNA copy number was determined in each sample by the ratio between the amount of a fragment of the *mitochondrial cytochrome B* (*mito CytB*) and the amount of the *beta-2-microglobulin* (*B2m*) nuclear gene, using the CFX96 Manager software (v. 3.0; Bio-Rad).

2.14. Analysis of gene expression

Total RNA was extracted with Aurum total RNA mini kit (Bio-Rad), following manufacturer's protocols, and quantified using a Nanodrop 2000 (ThermoScientific, Waltham, MA, USA), confirming that A260/280 was higher than 1.9. RNA integrity was verified by Experion RNA StdSens kit (Bio-Rad, Hercules, CA, USA), and RNA was converted into cDNA using the iScript cDNA synthesis kit (Bio-Rad), following manufacturer's instructions. RT-PCR was performed using the SsoFast Eva Green Supermix, in a CFX96 real time-PCR system (Bio-Rad, Hercules, CA, USA), with the primers defined in Table 2, at 500 nM. Amplification of 25 ng was performed with an initial cycle of 30 s at 95 °C, followed by 40 cycles of 5 s at 95 °C plus 5 s at 60 °C. At the end of each cycle, Eva Green fluorescence was recorded to enable determination of Cq. After amplification, melting temperature of the PCR products was determined by performing melting curves and amplicon length was confirmed by agarose electrophoresis. For each set of primers, amplification efficiency was assessed, and no template and no transcriptase controls were run. Gene expression was normalized to the geometric mean of RNA levels of 4 reference genes, including *mitochondrial 37S ribosomal protein* (*MRPL51*), *hypoxanthine phospphoribosyltransferase 1* (*HPRT1*), *C19orf74*, and *family with sequence similarity 57 member A* (*FAM57A*) by using the CFX96 Manager software (v. 3.0; Bio-Rad).

2.15. Measurement of lysosomal proteolytic capacity

Lysosomal proteolytic capacity [26,27] was measured using the DQ Red BSA Dye (Molecular Probes) following manufacturer's protocol. Briefly, 1 mg of dye was resuspended in 1 mL of PBS 1× and 100 μL of the resuspended dye was added to 10 mL of warm HGm. Previously seeded cells at density of 15,000 cells/cm^2 in white opaque-bottom, 96-well plates, cultured at least overnight after seeding, were loaded with 100 μL per well each of the dye-containing medium and incubated at 37 °C for 1 h. Cells were then washed twice with warm PBS 1× and the medium was replaced with 100 μL/well of warm EBSS medium (14155063, Thermo Scientific). The kinetics of DQ Red BSA digestion were recorded at respective excitation and emission maxima of 590 nm and 620 nm in a microplate reader over a 4 h period.

2.16. Computational data analysis

The computational analysis of the data was performed using Python 3, version 3.7.3. We relied on the Pandas [28] and SciPy [29] packages to load, store, transform, and perform a statistical analysis of the data. Correlation matrices and cluster map plots were created using Matplotlib [30] and Seaborn modules [31]. Estimation of the information gain was obtained with Orange Biolab [32].

The Pearson coefficient was adopted to estimate the correlation between pairs of variables. Values belong to the interval $[-1, 1]$, where $+1$ (respectively, -1) signals a total positive (respectively, negative) linear correlation and 0 identifies the nonexistence of linear correlation. The estimation of the mutual information between each individual feature and the target was calculated with the information gain measure, i.e., by estimating decrease of entropy [33].

Cluster maps relate features (in columns) with instances (in rows). The color of each cell represents the normalized level of expression of a particular feature in a specific instance. A two-way hierarchical clustering method groups the information displayed both in rows and in columns. The squared Euclidean distance metric was adopted for all cladograms presented in this work.

2.17. Statistical analysis

Data were analyzed using GraphPad Prism 6.01 (GraphPad Software, Inc. San Diego, CA, USA) and all results were expressed as mean ± standard error of the mean (SEM) for the number of experiments indicated in the legends of the figures. After assessing data normality with Kolmogorov-Smirnov and Shapiro-Wilk tests, statistical analysis of two groups was performed using the non-parametric Mann-Whitney test. Statistical analysis of three or more groups was performed using one-way analysis of variance (ANOVA) followed by a Sidak post hoc test for comparing different mitochondrial poisons concentrations. Values with $p < 0.05$ were considered as statistically significant (*).

3. Results

3.1. Human skin fibroblasts from sporadic PD patients have hyperpolarized and elongated mitochondrial networks

We performed an initial cell proliferation measurement, in order to select the appropriate cell density to perform long-term (96 h) assays, confirming that cells were still in exponential growth phase. Fibroblasts from sPD patients (Supplementary Fig. 1B) and their sex- and age-matched controls (Supplementary Fig. 1A) cultured in HGm were plated at different cell densities (1000; 2500; 5000; 10,000; 15,000; and 20,000 cells/cm^2) and several time points were used for following cell proliferation (24, 48, 72, and 96 h). Our results showed that cells proliferated linearly for 96 h at least when plated at 15,000 cells/cm^2 (Supplementary Fig. 1A and B). With the exception of vital fluorescence microscopy measurements, all the experiments were performed using this cell density.

Mitochondrial dysfunction has been shown in several PD models [5,14,34]. To evaluate mitochondrial network morphology and Δψmt in fibroblasts from sPD patients, we used vital epifluorescence imaging of cells loaded with the Δψmt-sensitive fluorescent probe TMRM. We observed an increase in TMRM fluorescence in fibroblasts from sPD patients (Fig. 1A and B), along with more elongated mitochondria (Fig. 1C) while mitochondrial interconnectivity (Fig. 1D) was not altered.

Mitochondrial morphology is an actively regulated and dynamic feature modulated by mitochondrial fusion, fission, and biogenesis. We next evaluated total content of proteins involved in mitochondrial fusion (OPA1) and fission (FIS and p-DRP1 ser 637) by using Western blotting; however, no differences were observed (Supplementary Fig. 2). We also measured metabolic viability using resorufin fluorescence, intracellular ATP levels using CellTiter-Glo luminescent cell viability assay, mtDNA copy number using RT-PCR, and lysosomal proteolytic capacity using DQ red BSA dye assay, as described in the Materials and methods section. Intracellular ATP levels were decreased in fibroblasts from sPD patients (Fig. 1F), while no alterations were observed in cellular metabolic activity (Fig. 1E), mtDNA copy number (Fig. 1G), and lysosomal proteolytic capacity (Fig. 1H). Rotenone, an inhibitor of mitochondrial complex I, is used so far because rotenone-induced toxicity mimics PD pathology [35]. Using SRB assay, susceptibility of control and fibroblasts from sPD patients to complex I inhibitor by rotenone was also tested. We show that fibroblasts from sPD patients were more susceptible to lower rotenone concentrations when treated for 24 h (Fig. 1I) and 48 h (Fig. 1J) compared to control fibroblasts.

3.2. Human skin fibroblasts from sporadic PD patients have higher mitochondrial oxidative stress

Increased mitochondrial oxidative stress is associated with several diseases, including PD [36,37]. We measured mitoSOX fluorescence in order to evaluate mitochondrial oxidative stress as described in the Materials and methods section. Fig. 2A shows that fibroblasts from sPD patients showed higher mitoSOX fluorescence, reflecting an oxidizing mitochondrial environment. The oxidative stress can be induced by an imbalance between oxidants and antioxidants. Other than the overproduction superoxide, we also assessed total SOD activity and mRNA levels for the two antioxidant enzymes, superoxide dismutase 1 and 2

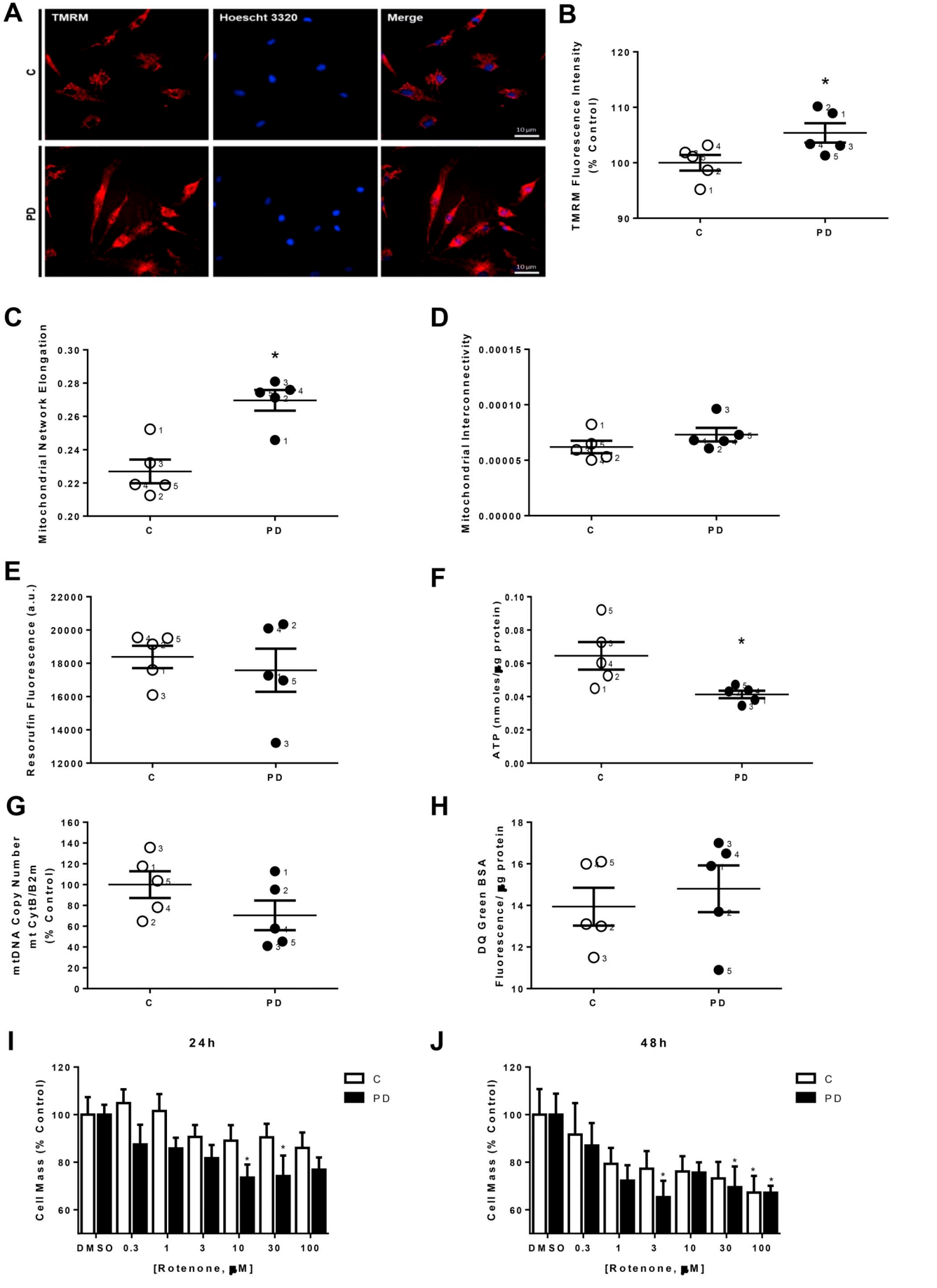

(caption on next page)

Fig. 1. Human skin fibroblasts from sporadic PD patients cultured in HGm presented hyperpolarized and elongated mitochondria, and lower levels of ATP. Cells were cultured in 25 mM glucose (HGm) and incubated for 30 min with fluorescent probes, TMRM (100 nM), and Hoescht 33342 (1 mg/mL) (A) as described in the Materials and methods section. TMRM intensity fluorescence of human skin fibroblasts from sPD (denoted as PD) and their matched-controls (denoted as C) were measured by microscopy (B). The quantification of TMRM fluorescence was obtained by ImageJ 1.45S program. Graphic is expressed as mean ± SEM of TMRM intensity fluorescence divided by area. Mitochondrial elongation and interconnectivity of the same fluorescent cells were measured using an ImageJ macro [22] (n = 45 cells per group) (C and D). Metabolic activity was evaluated using resazurin assay after 5 h of incubation with resazurin (E). Intracellular ATP levels were measured by using CellTiter-Glo Luminescent Cell Viability Assay (Promega) following manufacturer's instructions (F). Total DNA was extracted, and amplified by real-time RT-PCR. Mitochondrial DNA copy number was normalized to *B2m* levels (G). Lysosomal proteolytic capacity was measured using DQ-Green BSA assay kit (Molecular probes) (H). Cells were incubated with different concentrations of rotenone (mitochondrial complex I inhibitor) for 24 h (I) and 48 h (J). Each datapoint corresponds to one different individual out of five in each group. Data are expressed as mean ± SEM of fibroblasts from 5 sPD patients and 5 respective age- and sex-matched healthy controls. *p < 0.05 denotes a significant difference from control (C) or a significant difference from the same cell line incubated with the maximum volume of rotenone vehicle (DMSO).

(SOD1 and SOD2). No differences were observed in total SOD activity between fibroblasts from sPD patients and control fibroblasts (Fig. 2B), nor was alteration in the transcript expression for SOD1 and SOD2 (Fig. 2C and D).

To further characterize the mitochondrial impact of fibroblasts from sPD patients, we compared the levels of several mitochondria-related transcripts with control fibroblasts using RT-PCR. However, no statistical significance was observed in gene expression of *NADH-ubiquinone oxidoreductase subunit A9* (*NDUFA9*) (Fig. 3A), *succinate dehydrogenase complex flavoprotein subunit A* (*SDHA*) (Fig. 3B), *ubiquinol-cytochrome c reductase core protein 2* (*UQCRC2*) (Fig. 3C), *cytochrome c* (*CYTC*) (Fig. 3D), *cytochrome c oxidase subunit 4i1* (*Cox4i1*) (Fig. 3E), *ATP synthase membrane subunit c locus 1* (*ATP5G1*) (Fig. 3F), *nuclear respiratory factor 1* (*NRF1*) (Fig. 3G), *nuclear factor erythroid 2 like 2* (*NFE2L2*) (Fig. 3H), *PTEN-induced kinase 1* (*PINK1*) (Fig. 3I), *mitofusin 1* (*MFN1*) (Fig. 3J), and *mitofusin 2* (*MFN2*) (Fig. 3K). Following this, our objective was to characterize the metabolic phenotype of fibroblasts from sPD patients and control fibroblasts in terms of mitochondrial OCR and ECAR, the former being an indirect measurement of glycolytic activity. We determined ECAR and OCR normalized by cell mass using the Seahorse XF^{e}96 Extracellular Flux Analyzer. Regarding ECAR analysis, we observed that basal glycolysis-related ECAR (Fig. 4A and B) was decreased in fibroblasts from sPD patients, while no alterations were observed in glycolytic capacity (Fig. 4A and C). Regarding OCR analysis, no alterations were found in basal respiration (Fig. 4D and E), maximal respiration (Fig. 4D and F), and ATP production-associated

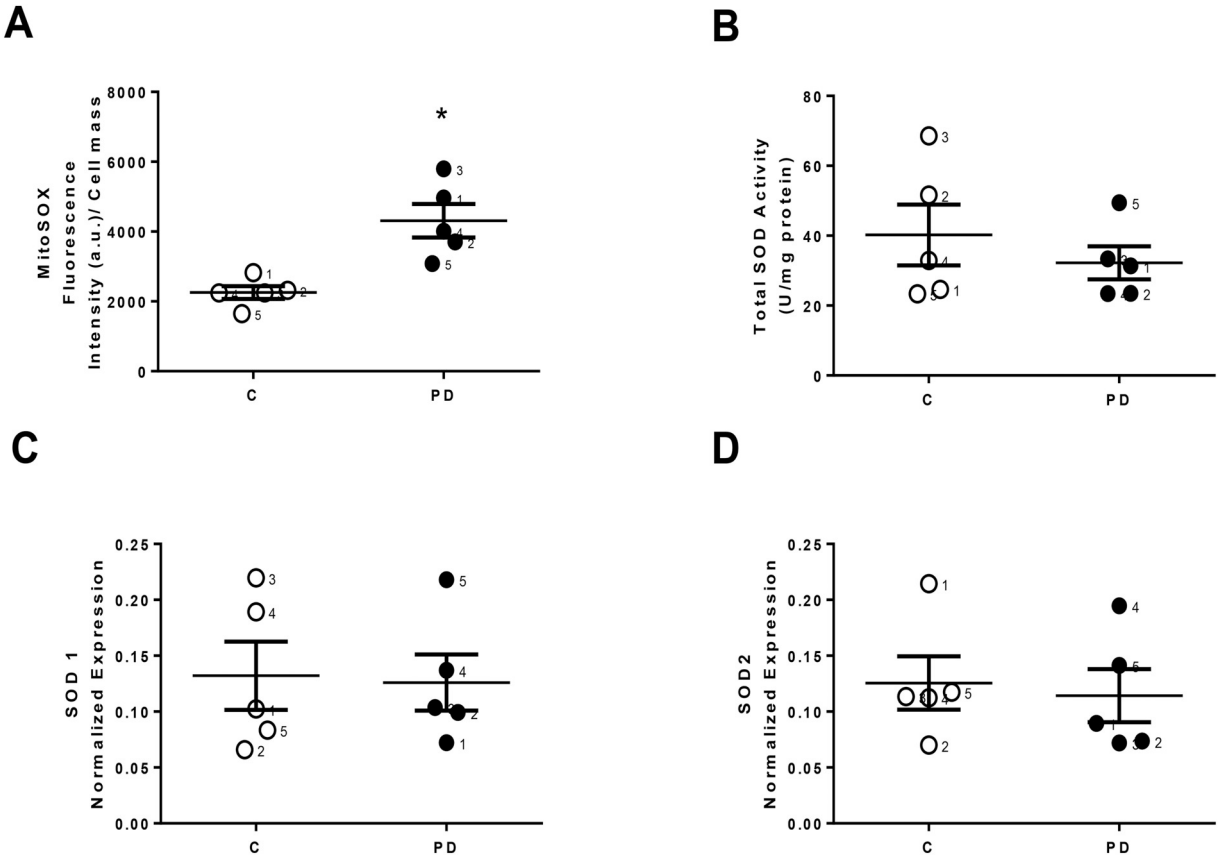

Fig. 2. Mitochondrial superoxide anion was increased in skin fibroblasts from sporadic PD patients cultured in HGm. Cells were cultured in 25 mM glucose (HGm) as described in the Materials and methods section. MitoSOX fluorescence was evaluated after 20 min incubation with MitoSOX fluorescent probe using a multi-well plate reader (A). Total superoxide dismutase (SOD) activity (B) was measured using a commercially available kit, following manufacturer's instructions. Total RNA was extracted, converted into cDNA, and amplified by real-time RT-PCR. Gene expression of *superoxide dismutase 1* (*SOD1*) (C) and *2* (*SOD2*) (D) were measured. Gene expression was normalized to geometric mean of 4 housekeeping genes, including *mitochondrial 37S ribosomal protein* (*MRPL51*), *hypoxanthine phosphoribosyltransferase 1* (*HPRT1*), *C19orf74*, and *family with sequence similarity 57 member A* (*FAM57A*) RNA levels. Each datapoint corresponds to one different individual out of five in each group. Data are expressed as mean ± SEM of fibroblasts from 5 sPD patients and 5 respective age- and sex-matched healthy controls. *p < 0.05 and **p < 0.01 denote a significant difference from control (C).

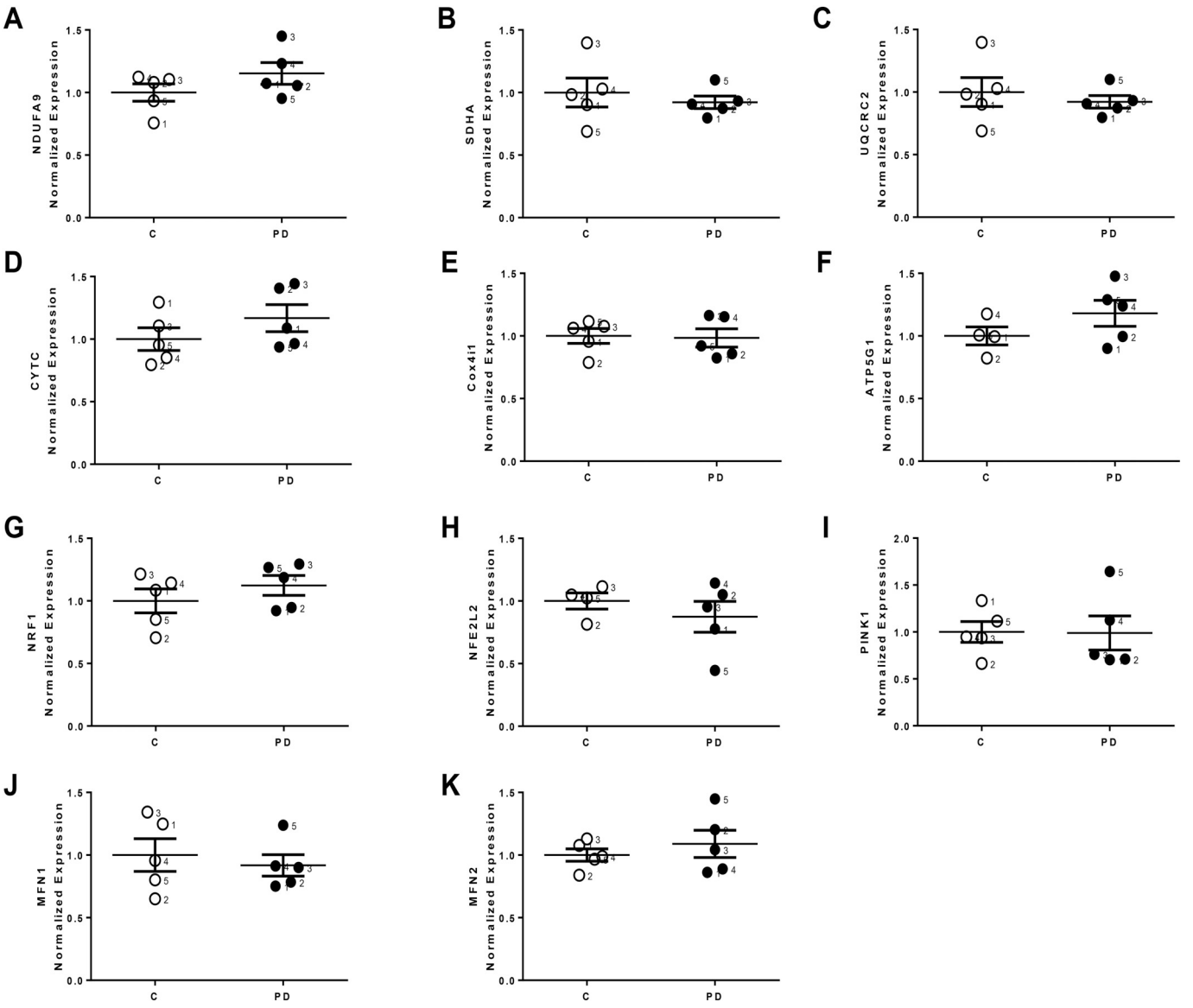

Fig. 3. Mitochondrial respiratory chain subunits-, dynamics-, and oxidative stress-related gene expression were not altered in skin fibroblasts from sporadic PD patients cultured in HGm. Cells were cultured in 25 mM glucose (HGm), as described in the Materials and methods section. Total RNA was extracted, converted into cDNA, and amplified by real-time RT-PCR. Gene expression of mitochondrial respiratory chain subunits (A to F), oxidative stress (G and H), and mitochondrial dynamics (I to K) were measured. Gene expression was normalized to the geometric mean of 4 housekeeping genes, including *mitochondrial 37S ribosomal protein* (*MRPL51*), *hypoxanthine phosphoribosyltransferase 1* (*HPRT1*), *C19orf74*, and *family with sequence similarity 57 member A* (*FAM57A*) RNA levels. Each datapoint corresponds to one different individual out of five in each group. Data are expressed as mean ± SEM of fibroblasts from 5 sPD patients and 5 respective age- and sex-matched healthy controls. *$p < 0.05$ denotes a significant difference from control (C).

OCR (Fig. 4D and G).

To better understand how the results obtained in HGm are related to each other, and to investigate whether these parameters allow for a clear separation between fibroblasts from control and sPD patients, we performed a computational data analysis methodology as described in the Materials and methods section. A correlation analysis of experimental end-points obtained so far revealed that the profiles of fibroblasts from sPD patients cultured in HGm are very different from those of control fibroblasts (Fig. 5A–B). At this point, the experimental end-points that allowed for a better distinction between controls and fibroblasts from sPD patients were found to be basal respiration, ATP-linked OCR, and mitochondrial superoxide anion (Fig. 5C). However, hierarchical clustering was not able to create a perfect separation of controls and fibroblasts from sPD patients for any of the three groups of features defined (Fig. 5D–F).

3.3. Mitochondrial remodeling of human skin fibroblasts from sporadic PD patients uncovered abnormalities in mitochondrial function

Mitochondrial complex I deficiency has been shown to occur in several PD models [38,39]. In our experiments performed in HGm, minor differences were found in most of the biological end-points measured in fibroblasts from sPD patients. However, rotenone sensitivity was higher in fibroblasts from sPD patients (Fig. 1I and J). Therefore, we hypothesized that fibroblasts from sPD patients could have a greater mitochondrial susceptibility, and so forcing fibroblasts from sPD patients to obtain most of their ATP through OXPHOS could uncover these dissimilarities in metabolic and signaling pathways when compared to control fibroblasts. Marroquin et al. [17] used a glucose-free/galactose/glutamine/pyruvate-containing culture medium to force HepG2 cells to use OXPHOS for most of ATP production, unmasking drug-induced mitochondrial toxicity. This approach was also used by

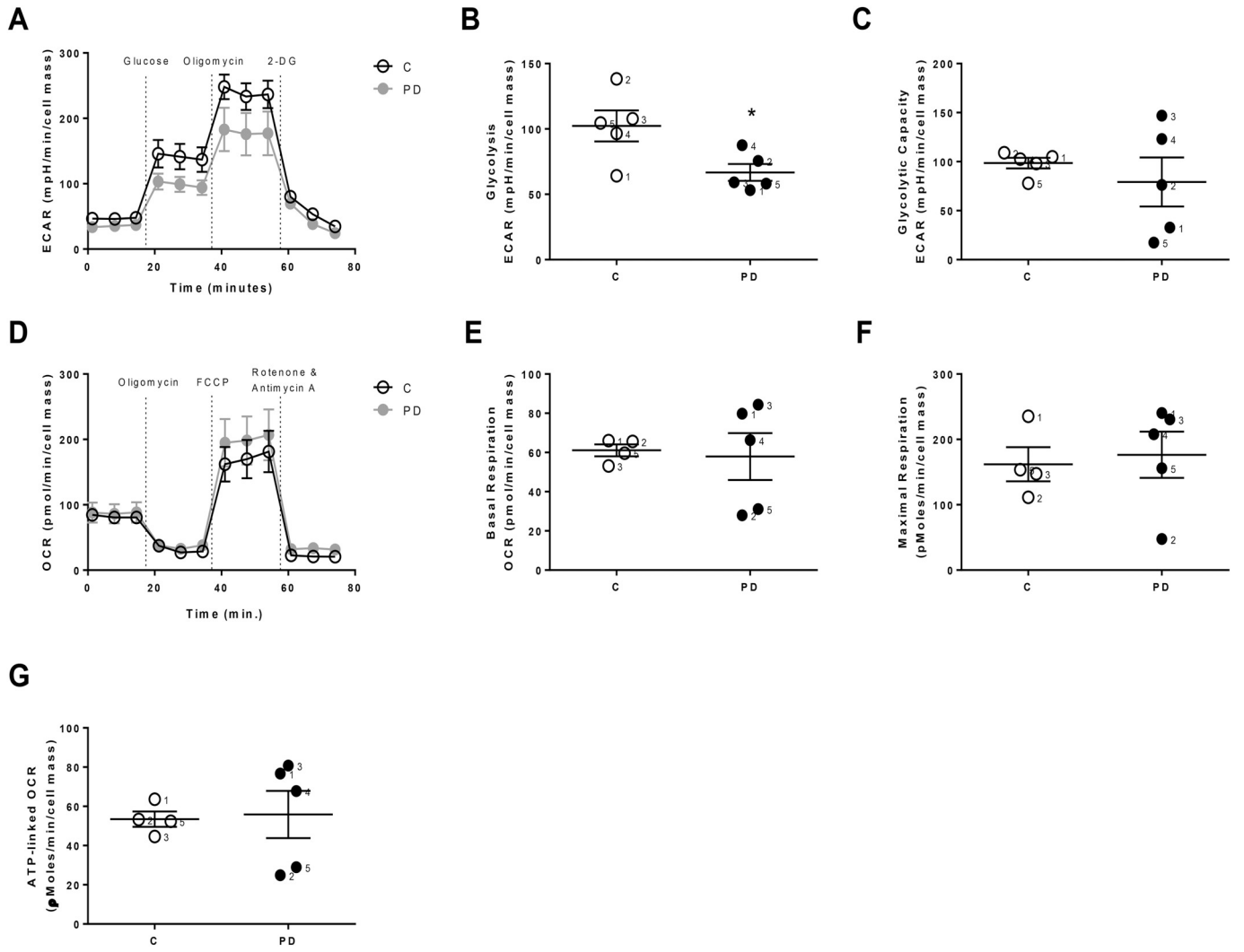

Fig. 4. Glycolysis-linked ECAR was decreased in skin fibroblasts from sporadic PD patients cultured in HGm. Cells were cultured in 25 mM glucose (HGm), as described in the Materials and methods section. The Seahorse XF^{e}96 Extracellular Flux Analyzer was used to measure Extracellular Acidification Rate (ECAR) (A to C) and Oxygen Consumption Rate (OCR) (D to G). Several ECAR parameters were evaluated: glycolysis (B) and glycolytic capacity (C). Several OCR parameters were evaluated: cell basal respiration (E), cell maximal respiration (F), and ATP production-linked OCR (G). Each datapoint corresponds to one different individual out of five in each group. Data are expressed as mean ± SEM of fibroblasts from 5 sPD patients and 5 respective age- and sex-matched healthy controls. *$p < 0.05$ denotes a significant difference from control (C).

our group to perform a metabolic and phenotypic characterization of human skin fibroblasts [25]. Based on that, we evaluated OCR in fibroblasts from sPD patients using the Seahorse XF^{e}96 Extracellular Flux Analyzer, after cellular adaptation to OXPHOSm, as previously described by Marroquin and us [17,25]. Surprisingly, no differences in OCR between fibroblasts from sPD patients and control fibroblasts were observed, when cells were cultured with the classic OXPHOSm adaptation protocol, in which at least 5 passages in OXPHOSm were performed before the experiments (Supplementary Fig. 3A, B, C, and D). Assuming that OXPHOS-defective cells could be lost during the adaptation protocol, which includes several passages, we performed incubation with the OXPHOSm for 1, 6, and 24 h, without passing cells. We demonstrated that after 24 h of incubation with OXPHOSm, fibroblasts from sPD patients presented overall decreased OCR, including reduced basal respiration (Fig. 6A and B), smaller proton leak (Fig. 6A and C), diminished maximal respiration (Fig. 6A and D), declined spare respiratory capacity (Fig. 6A and E), and lower ATP production-associated OCR (Fig. 6A and F), concomitant with lower intracellular ATP levels (Fig. 6G). Although nothing much changed after 1 h of OXPHOSm incubation (Supplementary Fig. 3E, F, G, and H), after 6 h of incubation with OXPHOSm, fibroblasts from sPD patients showed decreased basal respiration (Supplementary Fig. 3I and J) and maximal respiration (Supplementary Fig. 3I and K), while no alterations in ATP production-associated OCR were observed (Supplementary Fig. 3I and L). With these results, we conclude that 24 h of OXPHOSm incubation was the best approach to uncover mitochondrial abnormalities present in fibroblasts from sPD patients, which were hidden when cells were cultured in HGm. Using this approach, we also evaluated intracellular ATP levels using CellTiter-Glo luminescent cell viability assay as described in the Materials and methods section. As expected, fibroblasts from sPD patients had lower intracellular ATP levels (Fig. 6G). Moreover, we also measured the proliferation rates of 24 h of fibroblasts from sPD patients and their sex- and age-matched controls cultured in HGm or OXPHOSm for 9 days. Our results showed that cells were actively proliferating when cultured in HGm or OXPHOSm and that fibroblasts submitted to the OXPHOSm presented a proliferation profile similar to cells cultured in HGm, suggesting an effective adaptation to a more oxidative metabolism that supports the proliferation in OXPHOSm (Supplementary Fig. 1C and D).

Afterwards, we evaluated mitochondrial network morphology and $\Delta\psi$mt using vital epifluorescence imaging of OXPHOSm-cultured cells loaded with the $\Delta\psi$mt-sensitive fluorescent probe TMRM. We noted

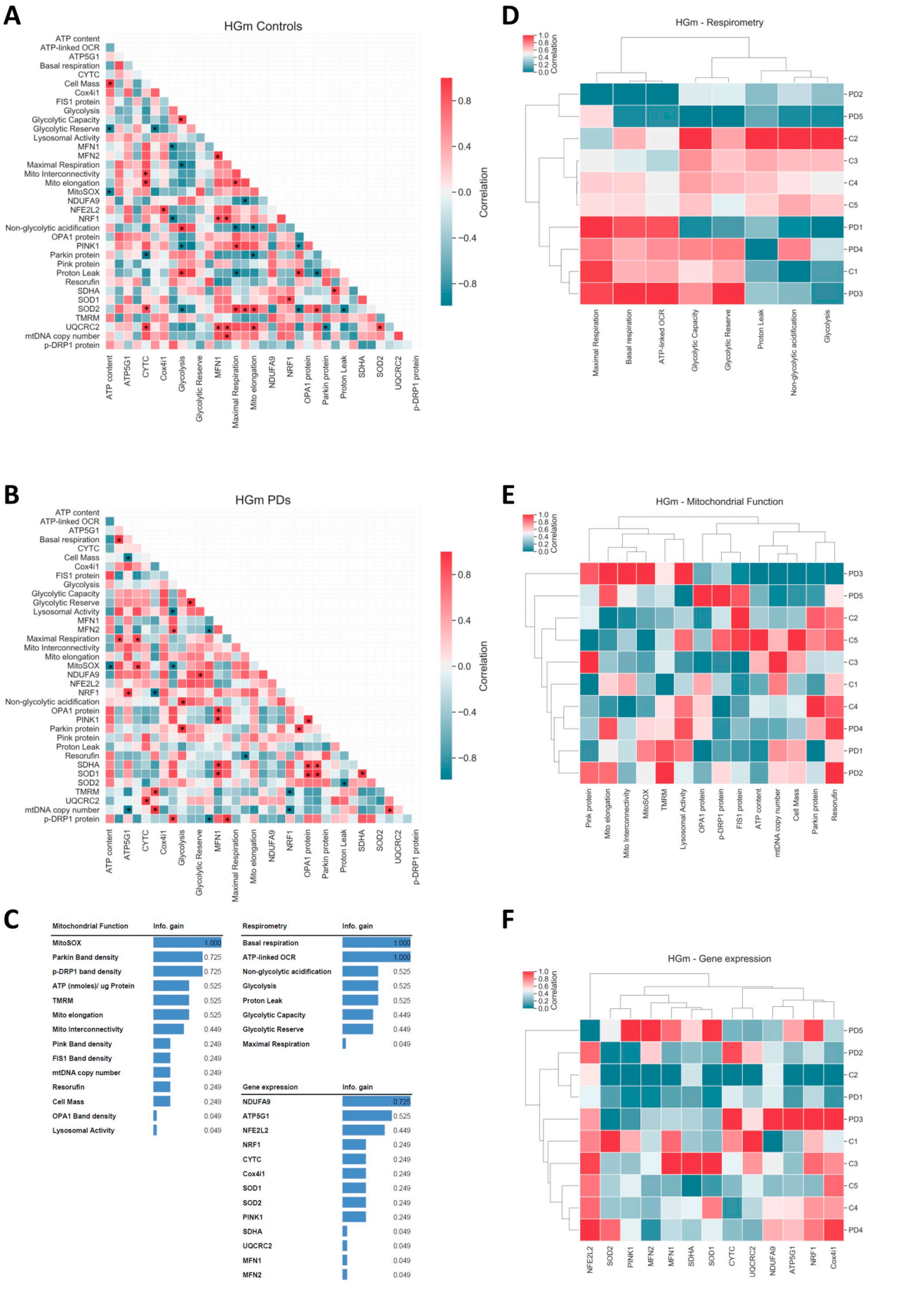

(caption on next page)

Fig. 5. Integrative analysis of all experimental end-point measures analyzed in fibroblasts from sPD patients and their matched controls cultured in HGm. A–B) Correlation matrices for A) control and B) PD cells. For better visualization, experimental end-point measures were subdivided into 3 groups: Gene Expression, Respirometry, and Other Mitochondrial Features. C) Information gain of each experimental end-point measured. D–F) Cluster maps relating features (experimental end-point measures) and samples (fibroblasts from sPD patients and their matched controls), for each of the three groups considered. Hierarchical clustering of the features and the samples was performed using the squared Euclidean distance metric. *p < 0.05 denotes a significant difference between groups.

that TMRM fluorescence was higher in fibroblasts from sPD patients (Fig. 7A and B). We then measured cell viability using resorufin fluorescence, mtDNA copy number using RT-PCR, and mitochondrial oxidative stress and total SOD activity using SOD activity kit assay. Our results show that fibroblasts from sPD patients presented decreased cell viability (Fig. 7C), concomitant with increased mitoSOX fluorescence, indicating increased superoxide or mitochondrial ROS production (Fig. 7E). Moreover, no differences were observed in total SOD activity content (Fig. 7F), GSH/GSSG ratio (Fig. 7G), and mtDNA copy number (Fig. 7D) in fibroblasts from sPD patients.

3.4. Phosphorylation of DRP1 at serine 637 was increased in human skin fibroblasts from sporadic PD patients

Mitochondrial dynamics are tightly regulated by fusion and fission events. Dysfunctional mitochondrial dynamics can lead to the accumulation of abnormal mitochondria, contributing to cellular damage, and have already been associated with PD pathogenesis [40,41]. We evaluated total protein content of mitochondrial fusion (OPA1) and fission (FIS1 and p-DRP1 Ser 637) by using Western blotting. We observed that fibroblasts from sPD patients showed increased p-DRP1 Ser 637 protein content, while no alterations in OPA1 and FIS1 protein content were found (Fig. 8). Furthermore, several mutated genes have been linked to PD [42,43] and some of them are associated with mitochondria, such as PINK1 and Parkin [44,45], due to their involvement

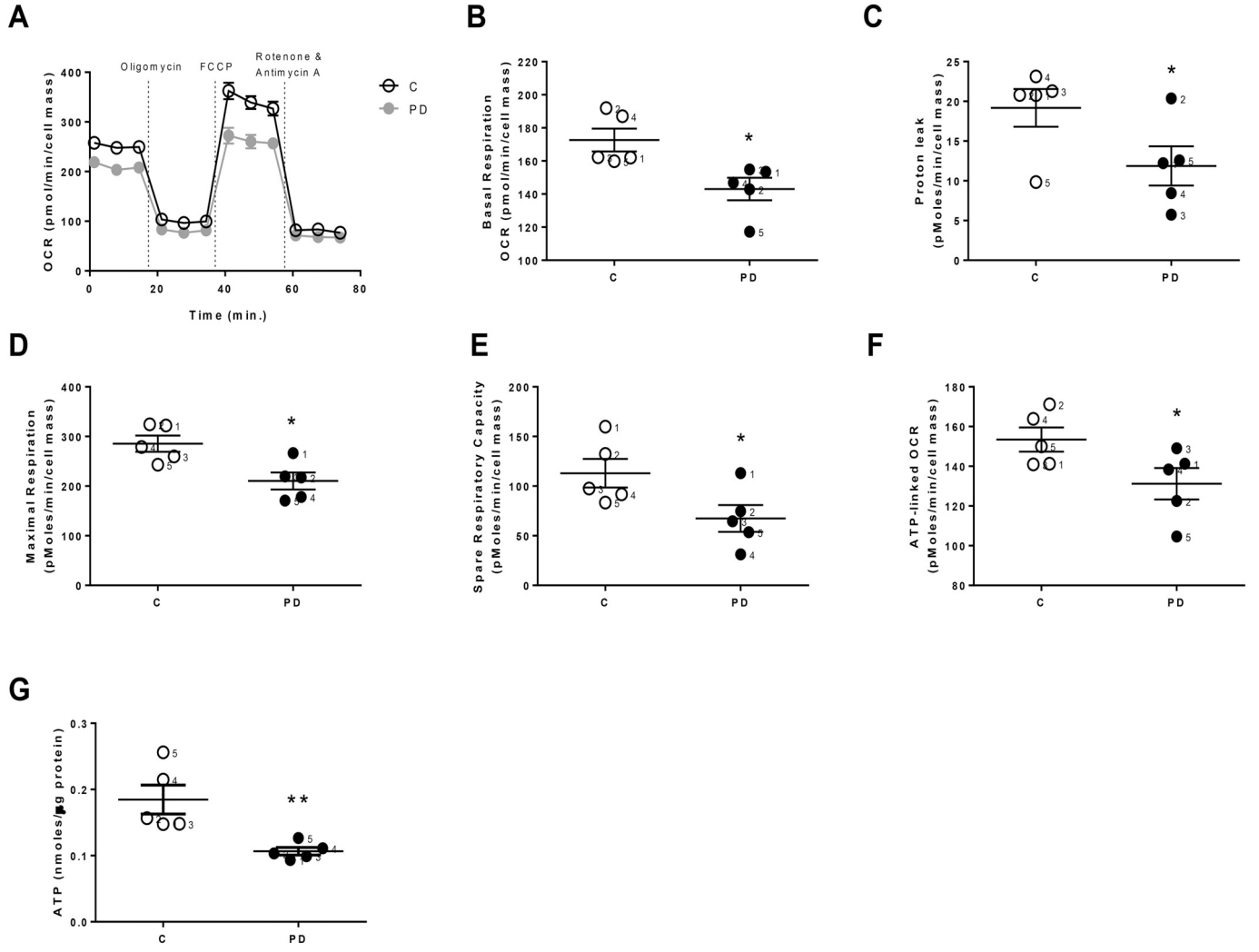

Fig. 6. Mitochondrial remodeling in skin fibroblasts from sporadic PD patients uncovers oxygen consumption rate (OCR) alterations. Cells were cultured in 5 mM glucose and 24 h after seeding, cell culture medium was changed to galactose/glutamine/pyruvate-containing medium (OXPHOSm), as described in the Materials and methods section. The Seahorse XF^{e}96 Extracellular Flux Analyzer was used to measure Oxygen Consumption Rate (OCR) (A). Several OCR parameters were evaluated: cell basal respiration (B), proton leak (C), cell maximal respiration (D), and ATP production-linked OCR (E). Intracellular ATP levels were measured by using CellTiter-Glo Luminescent Cell Viability Assay (Promega) following manufacturer's instructions (G). Each datapoint corresponds to one different individual out of five in each group. Data are expressed as mean ± SEM of fibroblasts from 5 sPD patients and 5 respective age- and sex-matched healthy controls. *p < 0.05 and **p < 0.01 denote a significant difference from control (C).

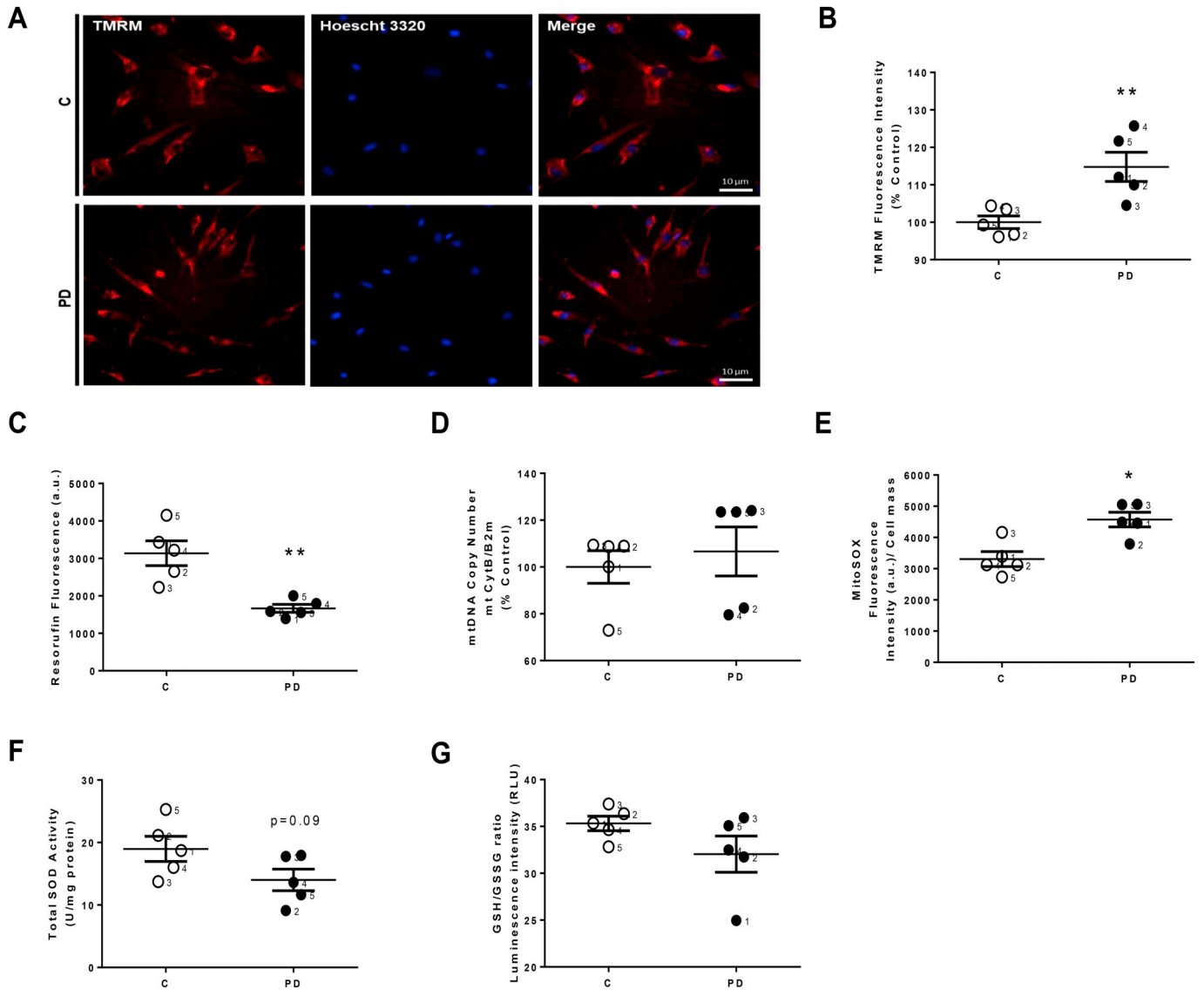

Fig. 7. Human skin fibroblasts from sporadic PD patients cultured in OXPHOSm presented hyperpolarized mitochondria and decreased metabolic activity. Cells were cultured in 5 mM glucose and 24 h after seeding, cell culture medium was changed to galactose/glutamine/pyruvate-containing medium (OXPHOSm), as described in the Materials and methods section. Thirty minutes before the end of the OXPHOSm incubation period, human skin fibroblasts were incubated with fluorescent probes, TMRM (100 nM) and Hoescht 33342 (1 mg/mL) (A). TMRM intensity fluorescence of human skin fibroblasts from sPD and their matched-controls were measured by microscopy (B). The quantification of TMRM fluorescence was obtained by ImageJ 1.45S program. Graphic is expressed as mean ± SEM of TMRM intensity fluorescence divided by area. Metabolic activity was evaluated using resazurin assay after 5 h of incubation with resazurin (C). Total DNA was extracted and amplified by real-time RT-PCR. Mitochondrial DNA copy number was normalized to *B2m* levels (D). MitoSOX fluorescence was evaluated after 20 min incubation with MitoSOX fluorescent probe using a multi-well plate reader (E). Total SOD activity (F) and GSH/GSSG ratio (G) were measured using commercially available kits (SOD activity Enzo Life Sciences and GSH/GSSG-Glo Assay [Promega], respectively) following manufacturer's instructions. Each datapoint corresponds to one different individual out of five in each group. Data are expressed as mean ± SEM of fibroblasts from 5 sPD patients and 5 respective age- and sex-matched healthy controls. *p < 0.05 and **p < 0.01 denote a significant difference from control (C).

in quality control mechanisms, including mitophagy [42]. Using the two approaches to culture cells (HGm and OXPHOSm), we measured total protein content of Parkin and PINK1 using Western blotting. Regardless of the cell culture approach used, no alterations in Parkin and PINK1 protein contents were observed between fibroblasts from sPD and control fibroblasts (Supplementary Fig. 4). However, when cells were cultured in HGm, there was a tendency towards a decrease in Parkin protein content in fibroblasts from sPD patients ($p = 0.09$) (Supplementary Fig. 4A).

The computational data analysis previously described was repeated to gain insight into the existing correlations of the OXPHOSm results and to investigate if these features allow for a clear separation between fibroblasts from sPD patients and healthy controls. The correlation analysis of experimental end-points taken in OXPHOSm revealed that the profiles of fibroblasts from sPD patients are very different from those of control fibroblasts (Fig. 9A–B). In this culture medium, the experimental end-point measures that allowed for a better distinction between control and PD fibroblasts were found to be basal respiration, ATP content, mitochondrial membrane potential, and metabolic activity (Fig. 9C). Importantly, hierarchical clustering was able to provide a perfect separation of controls and sPD patients fibroblasts based on the features measured in OXPHOSm (Fig. 9D).

4. Discussion

We showed here that metabolic and specifically mitochondrial

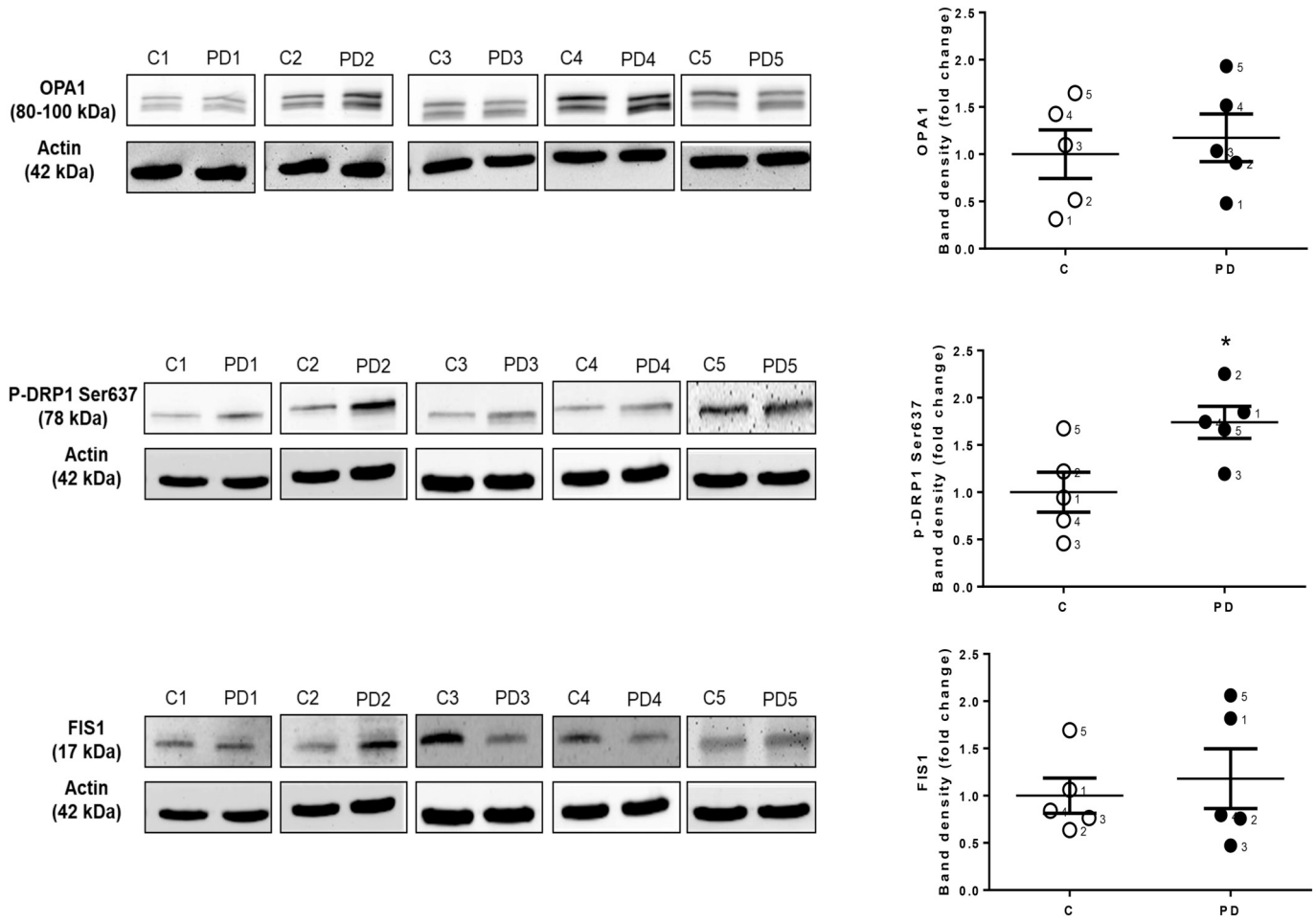

Fig. 8. Mitochondrial dynamics in skin fibroblasts from sporadic PD patients cultured forcing oxidative phosphorylation. Cells were cultured in 5 mM glucose and 24 h after seeding, cell culture medium was changed to galactose/glutamine/pyruvate-containing medium (OXPHOSm), as described in the Materials and methods section. Western blotting was used to detect mitochondrial dynamin-like GTPase OPA1, phosphorylation of dynamin-related protein 1 at Serine 637 (p-DRP1 Ser637), and mitochondrial fission 1 protein (FIS1) in total fractions from human skin fibroblast cell lines. Actin was used as loading control. Blots are representative of different cell preparations with a random distribution between C and PD. Each datapoint corresponds to one different individual out of five in each group. Data are expressed as mean ± SEM of fibroblasts from 5 sPD patients and 5 respective age- and sex-matched healthy controls. *$p < 0.05$ denotes a significant difference from control (C).

defects present in non-neuronal cells, such as fibroblasts from sPD patients, can be uncovered by using a modified culture medium which stimulates mitochondrial ATP production in order to cope with cell demands (Fig. 10). Importantly, clustering analysis of the experimental end-points in OXPHOSm resulted in a perfect separation of control and sPD fibroblasts. Thus, fibroblasts from sPD patients are an important tool to measure metabolic defects associated with PD pathogenesis. Since sPD pathophysiology can have diverse ethiologies, it is important to develop assays to determine particular mitochondrial defects and develop personalized therapeutic strategies. Considering that fibroblasts can be collected from patients in minimally-invasive ways, our work highlights the possibility of using individual fibroblasts from particular sPD patients and applying a metabolic remodeling strategy for taking into consideration the mitochondrial heteroplasmy when measuring drug treatment for personalized medicine. Measuring the individual mitochondrial response to chemical agents in fibroblasts from sPD patients can lead to significant savings in deterioration of patient health and shorten the time and cost for drug development.

Currently, PD is an incurable disease and no early diagnostic methods exist. Based on that, we hypothesized that fibroblasts from sPD male patients represent a minimally-invasive model to detect metabolic and mitochondrial alterations characteristic in PD patients, and that forcing mitochondrial oxidative phosphorylation reveals hidden metabolic alterations present in the same cells. It is known that mitochondrial dysfunction is an important feature of degenerating neurons in PD [46,47]. Moreover, it has been previously demonstrated that fibroblasts from PD patients have several typical characteristics present in neurons of PD patients, such as compromised mitochondrial structure and function, reduction in auto(mito)phagy, high levels of oxidative stress, and decreased capacity to activate the stress response [5,14,48]. Furthermore, PD fibroblasts showed higher vulnerability to necrotic cell death induced by rotenone, reduced UPS function, and decreased maximal and rotenone-sensitive mitochondrial respirations [5]. It is known that activation of cell death pathways depends on ROS production and ATP synthesis, which are regulated by mitochondrial transmembrane potential [49]. Similarly, we demonstrated here that mitochondria were hyperpolarized and elongated, ATP levels were decreased (Fig. 1), and mitochondrial ROS levels were increased in fibroblasts from sPD patients (Fig. 2), which can be early steps to trigger the apoptotic cell death pathway [49]. These alterations in fibroblasts from sPD patients are not related to decreases in antioxidant defenses, such as SOD (Fig. 2B–D), an important enzyme that catalyzes the dismutation of superoxide anion, which is confirmed by the unchanged GSH/GSSG ratio (Fig. 7G). Conversely, a compensatory upregulation of mitochondrial SOD, glutathione reductase, and glutathione-S-transferase levels were observed in fibroblasts from PD patients with

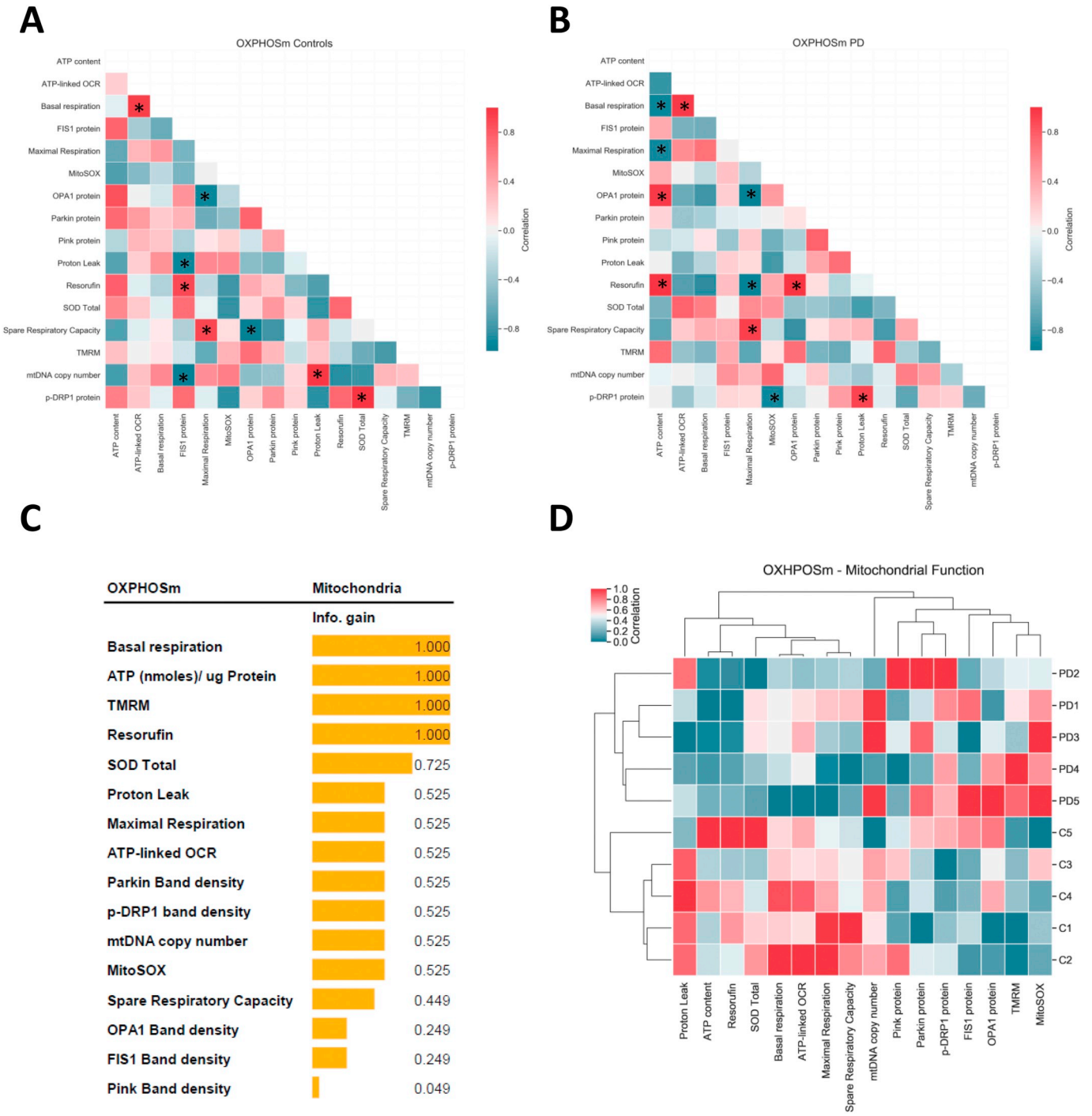

Fig. 9. Integrative analysis of all experimental end-point measures analyzed in fibroblasts from sPD patients and their matched controls cultured in OXPHOSm. A–B) Correlation matrices for A) control fibroblasts and B) fibroblasts from sPD patients. C) Information gain of each experimental end-point measured. D) Cluster map relating features (experimental end-point measures) and samples (patients). Hierarchical clustering of the features and the samples was performed using the squared Euclidean distance metric. *p < 0.05 denote a significant difference between groups.

homozygous PINK1 mutation [50], as were decreased SOD levels in blood cells from PD patients [7], which may serve as an adaptive response to increased oxidative stress. Superoxide anion is produced as a by-product of oxygen metabolism and, when over-produced, can lead to cell damage [50]. Surprisingly, only a decrease in ECAR-related glycolysis (Fig. 4A and B) was observed in fibroblasts from sPD patients, while no differences were observed in several mitochondria-related transcripts (Fig. 3) and mitochondrial bioenergetics assessed by OCR (Fig. 4D to G). These results could be due to the fact that these cells were cultured in HGm, mostly relying on glycolysis for ATP production [17], showing compromised metabolism of fibroblasts from sPD patients. In fact, disruption of the glycolytic pathway, including increased lactate levels, has been associated with several neurodegenerative disorders, such as PD [51]. Moreover, Smith, Depp et al. [7] showed that mitochondrial dysfunction was associated with a concomitant increase in glycolysis in peripheral blood mononuclear cells isolated from PD patients. Surprisingly, at this point, the measurements that allowed for a better distinction between control and sPD patients fibroblasts were found to be basal respiration, ATP-linked OCR, and mitochondrial superoxide anion (Fig. 5C), even when no conventional statistical

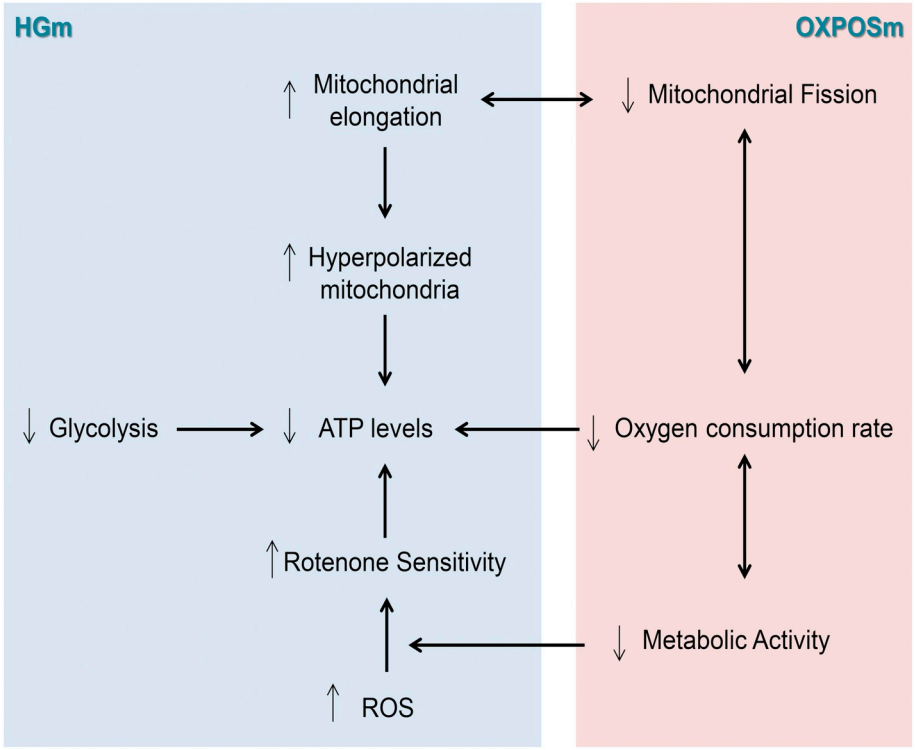

Fig. 10. Overview of the abnormalities present in human skin fibroblasts from sporadic PD patients when cultured in HGm and OXPHOSm. Human skin fibroblasts from sPD patients cultured in HGm showed hyperpolarized and elongated mitochondrial networks, higher mitochondrial ROS content, and decreased ATP levels and glycolysis-related ECAR. Moreover, sensitivity to rotenone, a mitochondrial complex I inhibitor, was higher in human skin fibroblasts from sPD patients. These abnormalities of fibroblasts from sPD patients became more evident when stimulating mitochondrial OXPHOS. Thus, forcing mitochondrial OXPHOS uncovers metabolic defects that were otherwise hidden, such as fibroblasts from sPD cells presenting decreased metabolic activity, basal respiration, ATP-linked OCR, and maximal respiration, and increased mitochondria-targeting phosphorylation of DRP1.

differences were found in these parameters when cells were cultured in HGm (Fig. 4D to F). Taking into account our results and the fact that rotenone (mitochondrial complex I inhibitor) sensitivity was higher in fibroblasts from sPD patients (Fig. 1I and J), as well as the fact that mitochondrial complex I defects are present in several PD models [38,39], we used a glucose-free and galactose/glutamine/pyruvate-containing culture medium (OXPHOSm) to force cells to use OXPHOS for mostly all ATP production [17], exposing metabolic and mitochondrial defects of fibroblasts from sPD patients, which could be hidden when cells were cultured in HGm. Recently, Milanese et al. used the same approach to show that mitochondrial function correlates with clinical severity in idiopathic PD [52]. The authors focused on statistical models and machine-learning procedures to describe the relationship between the different analyzed parameters and achieved unbiased grouping of patients on the basis of both clinical and laboratory measures [52]. Our results showed that when fibroblasts from sPD patients were incubated in OXPHOSm for 24 h, we observed a lower OCR, including basal respiration (Fig. 6A and B), proton leak (Fig. 6A and C), maximal respiration (Fig. 6A and D), spare respiratory capacity (Fig. 6A and E), and ATP production-associated OCR (Fig. 6A and F) when compared with control fibroblasts, showing a compromised bioenergetic profile. Surprisingly, no differences between fibroblasts from sPD patients and control individuals were observed in OCR, when cells were cultured using the classic OXPHOSm adaptation protocol (Supplementary Fig. 3A, B, C, and D) [17,25], probably because defective cells could be lost during this protocol. Regarding bioenergetic properties, it has been shown that maximal respiration decreased [5] and proton leak increased in fibroblasts from PD patients [14]; however, no differences were found in ATP-linked OCR [5,14]. The majority of alterations in bioenergetic profile in fibroblasts from PD patients were found in samples from familial PD patients [15,53]. In fact, hereditary PD samples could be advantageous for studying PD, although the higher prevalence of sporadic PD should be taken into consideration when studying pathological mechanisms and new treatment therapies for PD. Other mitochondrial dysfunction end-points, including mitochondrial superoxide and nitric oxide levels, were shown to be increased in fibroblasts from sPD patients, as well as alterations in mitochondrial fission and fusion proteins [15] culminating in altered cell death pathways [14,15]. Previously, it has been shown that the mitochondrial network was less interconnected due to increases in fusion protein MFN1 and OPA1, concomitant with a decrease in fission protein DRP1 in genetic PD patient-derived fibroblasts [15]. Conversely, we demonstrated that the mitochondrial network was elongated and DRP1 phosphorylation at serine 637 was increased in fibroblasts from sPD patients (Fig. 8), while no alterations were found in fusion protein content (Fig. 8). Phosphorylation of DRP1 at serine 637 promotes inhibition of fission, since it inhibits DRP1 enzyme activity and its translocation to mitochondria [54,55]. Alterations in mitochondrial fission can generate metabolically different types of mitochondria, which can decide the cell fate [56]. Mitochondrial dynamics are important for mitochondrial bioenergetics and regulation of cell death [56,57]. In fact, it was shown that the imbalance in mitochondrial fusion/fission events contributes to enlargement and degeneration of hippocampal mitochondria of scrapie-infected mice [58].

Several gene mutations associated with PD have important roles in mitochondria turnover and cell metabolism, including *Parkin* and *PINK1* genes [42,43]. Although no statistic differences were found in Parkin and PINK1 protein contents regardless of the cell culture media used, when considering the 10 groups of cells analyzed, we noted a higher variability in the corresponding band density in sPD samples than in control cells (Supplementary Fig. 4A), which was maintained when cells were cultured in OXPHOSm (Supplementary Fig. 4A). In the latter culture medium, an increase in band density was also observed in some of the sPD samples when compared to control cells. Although at present the reasons for this are unknown, Liu et al. [59] demonstrated that Parkin regulates glycolysis due to its effect in ubiquitin conjugation to pyruvate kinase M2 (PKM2), as shown after biochemical purification of the protein complex. On the other hand, Parkin plays a central role in mitochondrial homeostasis and mitophagy through tagging and ubiquitylating depolarized or damaged mitochondria for clearance [60,61], impacting cell metabolism. Despite no alterations being observed in proteolytic capacity of lysosome (Fig. 1H), the perturbation in mitochondrial function resulting in increased superoxide (Fig. 2A) and susceptibility to rotenone (Fig. 1I and J) appear before the lysosomal

function gets impaired [26,62,63], suggesting that a therapeutic strategy designed to maintain lysosomal function and/or preventing mitochondrial dysfunction could be reasonable therapeutic approaches for sporadic PD.

Supplementary data to this article can be found online at https://doi.org/10.1016/j.bbadis.2019.165615.

Authors' contributions

CMD performed the experiments and the collection, analysis, and interpretation of data, generated figures, and wrote the original draft. SPP conceived, designed, and helped to carry out some experiments. TCO designed some experiments and wrote part of the manuscript. TCO and FBP performed the computational analysis. NR and PJO wrote part of the manuscript, were responsible for funding acquisition, and supervised the study. All authors revised the final form of the manuscript.

Transparency document

The Transparency document associated this article can be found, in online version.

Declaration of competing interest

None of the authors has any conflict of interest. The funding agencies had no role in study design, data collection and analysis, decision to publish, or preparation of this document.

Acknowledgements

The work was funded by the Montepio Foundation under the project “An Epigenetic Engineering Approach to Reverse the Parkinson Disease Cell State (PD-state)” (CPD0028001; 2015). This work was also financed by the European Regional Development Fund (ERDF) through the Centro 2020 Regional Operational Programme under project CENTRO-07-ST24-FEDER-002008 and through the COMPETE 2020-Operational Programme for Competitiveness and Internationalisation, and by Portuguese national funds via FCT–Fundação para a Ciência e a Tecnologia, under project(s) PTDC/MED-FAR/29391/2017, POCI-01-0145-FEDER-016659, POCI-01-0145-FEDER-028607, POCI-01-0145-FEDER-029297, POCI-01-0145-FEDER-029391, and UID/NEU/04539/2019. CMD (SFRH/BD/100341/2014) was supported by FCT PhD fellowships and SPP (SFRH/BPD/116061/2016) was supported by a FCT Post-Doctoral fellowship. NR was supported by European Research Council Starting Grant 337327 MitoPexLyso and Deutsche Forschungsgemeinschaft SFB1190-P02. The authors are extremely grateful to Alexandra Holy for English proofreading and to the Biomaterials and Stem Cell-Based Therapeutics Laboratory for helping with microscopy assays.

References

[1] L.M. Bekris, I.F. Mata, C.P. Zabetian, The genetics of Parkinson disease, J. Geriatr. Psychiatry Neurol. 23 (2010) 228–242.
[2] F. Moisan, S. Kab, F. Mohamed, M. Canonico, M. Le Guern, C. Quintin, et al., Parkinson disease male-to-female ratios increase with age: French nationwide study and meta-analysis, J. Neurol. Neurosurg. Psychiatry 87 (2016) 952–957.
[3] C.A. Davie, A review of Parkinson’s disease, Br. Med. Bull. 86 (2008) 109–127.
[4] L.M. de Lau, M.M. Breteler, Epidemiology of Parkinson’s disease, Lancet Neurol. 5 (2006) 525–535.
[5] G. Ambrosi, C. Ghezzi, S. Sepe, C. Milanese, C. Payan-Gomez, C.R. Bombardieri, et al., Bioenergetic and proteolytic defects in fibroblasts from patients with sporadic Parkinson’s disease, Biochim. Biophys. Acta 1842 (2014) 1385–1394.
[6] I. Gonzalez-Casacuberta, D.L. Juarez-Flores, M. Ezquerra, R. Fucho, M. Catalan-Garcia, M. Guitart-Mampel, et al., Mitochondrial and autophagic alterations in skin fibroblasts from Parkinson disease patients with Parkin mutations, Aging (Albany NY) 11 (2019) 3750–3767.
[7] A.M. Smith, C. Depp, B.J. Ryan, G.I. Johnston, J. Alegre-Abarrategui, S. Evetts, et al., Mitochondrial dysfunction and increased glycolysis in prodromal and early Parkinson’s blood cells, Mov. Disord. 33 (2018) 1580–1590.
[8] M.C. Zanellati, V. Monti, C. Barzaghi, C. Reale, N. Nardocci, A. Albanese, et al., Mitochondrial dysfunction in Parkinson disease: evidence in mutant PARK2 fibroblasts, Front. Genet. 6 (2015) 78.
[9] A. Abeliovich, A.D. Gitler, Defects in trafficking bridge Parkinson's disease pathology and genetics, Nature. 539 (2016) 207.
[10] K.F. Winklhofer, C. Haass, Mitochondrial dysfunction in Parkinson’s disease, Biochim. Biophys. Acta 1802 (2010) 29–44.
[11] R. Banerjee, A.A. Starkov, M.F. Beal, B. Thomas, Mitochondrial dysfunction in the limelight of Parkinson’s disease pathogenesis, Biochim. Biophys. Acta 1792 (2009) 651–663.
[12] J.W. Langston, P. Ballard, J.W. Tetrud, I. Irwin, Chronic Parkinsonism in humans due to a product of meperidine-analog synthesis, Science. 219 (1983) 979–980.
[13] M.E. Johnson, L. Bobrovskaya, An update on the rotenone models of Parkinson’s disease: their ability to reproduce the features of clinical disease and model gene–environment interactions, NeuroToxicology. 46 (2015) 101–116.
[14] J.M.Y. Teves, V. Bhargava, K.R. Kirwan, M.J. Corenblum, R. Justiniano, G.T. Wondrak, et al., Parkinson’s disease skin fibroblasts display signature alterations in growth, redox homeostasis, mitochondrial function, and autophagy, Front. Neurosci. 11 (2017) 737.
[15] G.A. Smith, J. Jansson, E.M. Rocha, T. Osborn, P.J. Hallett, O. Isacson, Fibroblast biomarkers of sporadic Parkinson’s disease and LRRK2 kinase inhibition, Mol. Neurobiol. 53 (2016) 5161–5177.
[16] G. Auburger, M. Klinkenberg, J. Drost, K. Marcus, B. Morales-Gordo, W.S. Kunz, et al., Primary skin fibroblasts as a model of Parkinson’s disease, Mol. Neurobiol. 46 (2012) 20–27.
[17] L.D. Marroquin, J. Hynes, J.A. Dykens, J.D. Jamieson, Y. Will, Circumventing the Crabtree effect: replacing media glucose with galactose increases susceptibility of HepG2 cells to mitochondrial toxicants, Toxicol. Sci. 97 (2007) 539–547.
[18] R. Rossignol, R. Gilkerson, R. Aggeler, K. Yamagata, S.J. Remington, R.A. Capaldi, Energy substrate modulates mitochondrial structure and oxidative capacity in cancer cells, Cancer Res. 64 (2004) 985–993.
[19] F.S. Silva, I.G. Starostina, V.V. Ivanova, A.A. Rizvanov, P.J. Oliveira, S.P. Pereira, Determination of metabolic viability and cell mass using a tandem resazurin/sulforhodamine B assay, Curr. Protoc. Toxicol. 68 (2016) (2 24 21-22 24 15).
[20] V. Vichai, K. Kirtikara, Sulforhodamine B colorimetric assay for cytotoxicity screening, Nat. Protoc. 1 (2006) 1112–1116.
[21] S.P. Crouch, R. Kozlowski, K.J. Slater, J. Fletcher, The use of ATP bioluminescence as a measure of cell proliferation and cytotoxicity, J. Immunol. Methods 160 (1993) 81–88.
[22] I. Vega-Naredo, R. Loureiro, K.A. Mesquita, I.A. Barbosa, L.C. Tavares, A.F. Branco, et al., Mitochondrial metabolism directs stemness and differentiation in P19 embryonal carcinoma stem cells, Cell Death Differ. 21 (2014) 1560–1574.
[23] M.M. Bradford, A rapid and sensitive method for the quantitation of microgram quantities of protein utilizing the principle of protein-dye binding, Anal. Biochem. 72 (1976) 248–254.
[24] Y. Wang, Z. Zeng, J. Lu, Y. Wang, Z. Liu, M. He, et al., CPT1A-mediated fatty acid oxidation promotes colorectal cancer cell metastasis by inhibiting anoikis, Oncogene 37 (2018) 6025–6040.
[25] S.P. Pereira, C.M. Deus, T.L. Serafim, T. Cunha-Oliveira, P.J. Oliveira, Metabolic and phenotypic characterization of human skin fibroblasts after forcing oxidative capacity, Toxicol. Sci. 164 (2018) 191–204.
[26] L. Fernandez-Mosquera, K.F. Yambire, R. Couto, L. Pereyra, K. Pabis, A.H. Ponsford, et al., Mitochondrial respiratory chain deficiency inhibits lysosomal hydrolysis, Autophagy. (2019) 1–20.
[27] R. Marwaha, M. Sharma, DQ-red BSA trafficking assay in cultured cells to assess cargo delivery to lysosomes, Bio Protoc. 7 (2017).
[28] W. McKinney, Data structures for statistical computing in python, Proceedings of the 9th Python in Science Conference, vol. 445, 2010, pp. 51–56.
[29] E. Jones, T. Oliphant, P. Peterson, SciPy: open source scientific tools for python, Available at: http://scipy.org.
[30] J.D. Hunter, Matplotlib: a 2D graphics environment, Comput. Sci. Eng. 9 (2007) 90–95.
[31] M. Waskom, Seaborn: statistical data visualization. mwaskom/seaborn: v0.9.0 (version v0.9.0), Zenodo, 2018.
[32] J. Demsar, T. Curk, A. Erjavec, G. C, T. Hocevar, M. Milutinovic, et al., Orange: data mining toolbox in python, J. Mach. Learn. Res. 14 (2013) 2349–2353.
[33] J.R. Quinlan, Induction of decision trees, Mach. Learn. 1 (1986) 81–106.
[34] F. Wauters, T. Cornelissen, D. Imberechts, S. Martin, B. Koentjoro, C. Sue, et al., LRRK2 mutations impair depolarization-induced mitophagy through inhibition of mitochondrial accumulation of RAB10, Autophagy, 2019.
[35] C. Gunaydin, B. Avci, A. Bozkurt, M.E. Onger, H. Balci, S.S. Bilge, Effects of agomelatine in rotenone-induced Parkinson’s disease in rats, Neurosci. Lett. 699 (2019) 71–76.
[36] C. Henchcliffe, M.F. Beal, Mitochondrial biology and oxidative stress in Parkinson disease pathogenesis, Nat. Clin. Pract. Neurol. 4 (2008) 600.
[37] H.N. Nguyen, B. Byers, B. Cord, A. Shcheglovitov, J. Byrne, P. Gujar, et al., LRRK2 mutant iPSC-derived DA neurons demonstrate increased susceptibility to oxidative stress, Cell Stem Cell 8 (2011) 267–280.
[38] I.H. Flones, E. Fernandez-Vizarra, M. Lykouri, B. Brakedal, G.O. Skeie, H. Miletic, et al., Neuronal complex I deficiency occurs throughout the Parkinson’s disease brain, but is not associated with neurodegeneration or mitochondrial DNA damage, Acta Neuropathol. 135 (2018) 409–425.
[39] A.H. Schapira, J.M. Cooper, D. Dexter, P. Jenner, J.B. Clark, C.D. Marsden, Mitochondrial complex I deficiency in Parkinson’s disease, Lancet. 1 (1989) 1269.
[40] H.S. Choi, Y.G. Choi, H.Y. Shin, J.M. Oh, J.H. Park, J.I. Kim, et al., Dysfunction of mitochondrial dynamics in the brains of scrapie-infected mice, Biochem. Biophys.

Res. Commun. 448 (2014) 157–162.
[41] M.T. Lin, M.F. Beal, Mitochondrial dysfunction and oxidative stress in neurodegenerative diseases, Nature. 443 (2006) 787–795.
[42] E. Janda, C. Isidoro, C. Carresi, V. Mollace, Defective autophagy in Parkinson's disease: role of oxidative stress, Mol. Neurobiol. 46 (2012) 639–661.
[43] M.A. Nalls, N. Pankratz, C.M. Lill, C.B. Do, D.G. Hernandez, M. Saad, et al., Large-scale meta-analysis of genome-wide association data identifies six new risk loci for Parkinson's disease, Nat. Genet. 46 (2014) 989–993.
[44] A. Kumar, J. Tamjar, A.D. Waddell, H.I. Woodroof, O.G. Raimi, A.M. Shaw, et al., Structure of PINK1 and mechanisms of Parkinson's disease-associated mutations, Elife. 6 (2017).
[45] A.M. Pickrell, R.J. Youle, The roles of PINK1, parkin, and mitochondrial fidelity in Parkinson's disease, Neuron. 85 (2015) 257–273.
[46] M.R. Cookson, Parkinsonism due to mutations in PINK1, parkin, and DJ-1 and oxidative stress and mitochondrial pathways, Cold Spring Harb. Perspect. Med. 2 (2012) a009415.
[47] K.A. Malkus, E. Tsika, H. Ischiropoulos, Oxidative modifications, mitochondrial dysfunction, and impaired protein degradation in Parkinson's disease: how neurons are lost in the Bermuda triangle, Mol. Neurodegener. 4 (2009) 24.
[48] S.M.S. Yakhine-Diop, M. Niso-Santano, M. Rodriguez-Arribas, R. Gomez-Sanchez, G. Martinez-Chacon, E. Uribe-Carretero, et al., Impaired mitophagy and protein acetylation levels in fibroblasts from Parkinson's disease patients, Mol. Neurobiol. 56 (2019) 2466–2481.
[49] A. Perl, P. Gergely Jr., G. Nagy, A. Koncz, K. Banki, Mitochondrial hyperpolarization: a checkpoint of T-cell life, death and autoimmunity, Trends Immunol. 25 (2004) 360–367.
[50] H.H. Hoepken, S. Gispert, B. Morales, O. Wingerter, D. Del Turco, A. Mulsch, et al., Mitochondrial dysfunction, peroxidation damage and changes in glutathione metabolism in PARK6, Neurobiol. Dis. 25 (2007) 401–411.
[51] E.C. Schulte, E. Altmaier, H.S. Berger, K.T. Do, G. Kastenmuller, S. Wahl, et al., Alterations in lipid and inositol metabolisms in two dopaminergic disorders, PLoS One 11 (2016) e0147129.
[52] C. Milanese, C. Payan-Gomez, M. Galvani, N. Molano Gonzalez, M. Tresini, S. Nait Abdellah, et al., Peripheral mitochondrial function correlates with clinical severity in idiopathic Parkinson's disease, Mov Disord, 2019.
[53] B. Koentjoro, J.S. Park, C.M. Sue, Nix restores mitophagy and mitochondrial function to protect against PINK1/Parkin-related Parkinson's disease, Sci. Rep. 7 (2017) 44373.
[54] A. Jahani-Asl, R.S. Slack, The phosphorylation state of Drp1 determines cell fate, EMBO Rep. 8 (2007) 912–913.
[55] A.J. Roe, X. Qi, Drp1 phosphorylation by MAPK1 causes mitochondrial dysfunction in cell culture model of Huntington's disease, Biochem. Biophys. Res. Commun. 496 (2018) 706–711.
[56] T. Zhu, J.L. Chen, Q. Wang, W. Shao, B. Qi, Modulation of mitochondrial dynamics in neurodegenerative diseases: an insight into prion diseases, Front. Aging Neurosci. 10 (2018) 336.
[57] D.F. Suen, K.L. Norris, R.J. Youle, Mitochondrial dynamics and apoptosis, Genes Dev. 22 (2008) 1577–1590.
[58] X. Yang, Q. Shi, J. Sun, Y. Lv, Y. Ma, C. Chen, et al., Aberrant alterations of mitochondrial factors Drp1 and Opa1 in the brains of Scrapie experiment rodents, J. Mol. Neurosci. 61 (2017) 368–378.
[59] K. Liu, F. Li, H. Han, Y. Chen, Z. Mao, J. Luo, et al., Parkin regulates the activity of pyruvate kinase M2, J. Biol. Chem. 291 (2016) 10307–10317.
[60] D. Narendra, A. Tanaka, D.F. Suen, R.J. Youle, Parkin is recruited selectively to impaired mitochondria and promotes their autophagy, J. Cell Biol. 183 (2008) 795–803.
[61] C. Vives-Bauza, C. Zhou, Y. Huang, M. Cui, R.L. de Vries, J. Kim, et al., PINK1-dependent recruitment of Parkin to mitochondria in mitophagy, Proc. Natl. Acad. Sci. U. S. A. 107 (2010) 378–383.
[62] C.V. Diogo, K.F. Yambire, L. Fernandez Mosquera, F.T. Branco, N. Raimundo, Mitochondrial adventures at the organelle society, Biochem. Biophys. Res. Commun. 500 (2018) 87–93.
[63] L. Fernandez-Mosquera, C.V. Diogo, K.F. Yambire, G.L. Santos, M. Luna Sanchez, P. Benit, et al., Acute and chronic mitochondrial respiratory chain deficiency differentially regulate lysosomal biogenesis, Sci. Rep. 7 (2017) 45076.